THE EUROPEAN
PHYSICAL JOURNAL C

Flavor-dependent $U(1)$ extension inspired by lepton, baryon and color numbers

Duong Van Loi[a] , **Phung Van Dong**[b]

Phenikaa Institute for Advanced Study and Faculty of Basic Science, Phenikaa University, Yen Nghia, Ha Dong, Hanoi 100000, Vietnam

Abstract There is no reason why the gauge symmetry extension is family universal as in the standard model and the most well-motivated models, e.g. left-right symmetry and grand unification. Hence, we propose a simplest extension of the standard model – a flavor-dependent $U(1)$ gauge symmetry – and find the new physics insight. For this aim, the $U(1)$ charge, called X, is expressed as $X = xB + yL$ in which x and y are free parameters as functions of flavor index, e.g. for a flavor i they take x_i and y_i respectively, where B and L denote normal baryon and lepton numbers. Imposing a relation involved by the color number 3, i.e. $-x_{1,2,...,n} = x_{n+1,n+2,...,n+m} = 3y_{1,2,...,n+m} \equiv 3z$, for arbitrarily nonzero z, we achieve a novel $U(1)$ theory with implied X-charge. This theory not only explains the origin of the number of observed fermion families but also offers a possible solution for both neutrino mass and dark matter, which differs from $B - L$ extension. Two typical models based on this idea are examined, yielding interesting results for flavor-changing neutral currents and particle colliders, besides those of neutrino mass and dark matter.

1 Introduction

Although the standard model (SM) has been remarkably successful in describing the fundamental particles and interactions, it is known to be an incomplete theory and requires extension. Problems considered as limitations/shortcomings of the SM include the existence of dark matter which makes up most mass of galaxies and galaxy clusters in our universe [1], neutrino oscillations which require non-zero neutrino masses and flavor mixing [2,3], and specially why there are just three fermion families observed in the nature [4].

One of the most interesting extensions of the SM is an extra gauge symmetry $U(1)$ with associated gauge boson Z'. Such extension is well motivated since it not only occurs in grand unification and string theories but also supplies a new gauge dynamics which accounts the SM issues and experimental deviations [5], for instance, solution for dark matter [6–16], neutrino mass generation [17–21], muon anomalous magnetic moment [22–24], asymmetric matter production [25], and fermion family number [26,27]. It is stressed that this type of extension can be distinguished by Z' mass, Z'-fermion couplings, extended Higgs sector, possible couplings to a hidden sector, and kinetic mixing effect, etc.

In this work, we propose a flavor-dependent $U(1)$ extension of the SM, which has rarely been considered in the literature [28]. The $U(1)$ charge, labeled as X, has the form, $X = xB + yL$, where free parameters x and y take values x_i and y_i for flavor i, respectively, while B (L) denotes baryon (lepton) number, as usual. For brevity, we restrict the parameter space by assuming that only x_i depends on flavor i, whereas y_i does not, i.e. $y_i = z$ for all N_f families, where z is arbitrarily nonzero. Additionally, the x_i parameters are separated into two types of opposite signs, which relate to the parameter z via the color number 3, namely, $x_i = -3z$ for the first n families, while $x_i = 3z$ for the remaining m families, where $n + m = N_f$. Intriguingly, we obtain a novel $U(1)$ theory that not only requires the presence of right-handed neutrinos due to the anomaly cancellation (a framework for generating nonzero neutrino masses) but also leads to the number of fermion families to be a multiple of the color number, 3, i.e., $N_f = 3(n - m)$. It is noted that QCD asymptotic freedom requires $N_f \le 8$, which leads two solutions $N_f = 3$ and 6. Imposing the first solution $N_f = 3$ as observed, we obtain $n = 2$ and $m = 1$. Besides supplying a potential explanation to existence of three fermion families, this theory reveals possible answers for neutrino mass and dark matter. We will consider two realistic models recogniz-

[a] e-mail: loi.duongvan@phenikaa-uni.edu.vn (corresponding author)

[b] e-mail: dong.phungvan@phenikaa-uni.edu.vn

ing this feature. The first model, called conventional $U(1)_X$ model, predicts tiny neutrino masses via seesaw mechanism as well as scenario of a single dark matter. The second model, called alternative $U(1)_X$ model, provides a scenario of two-component dark matter, by contrast, while nonzero neutrino masses are induced by scotogenic mechanism. In addition, we will discuss interesting implications of each model for flavor-changing neutral currents (FCNCs) and particle colliders in detail.

The rest of this work is organized as follows: In Sect. 2, we consider anomaly cancellation conditions for the new gauge symmetry and arguments that lead to two realistic models. The implications of each model for neutrino mass and dark matter are presented in Sects. 3 and 4, respectively. In Sect. 5, we obtain constraints for each model from flavor-changing neutral currents and particle colliders. Dark matter phenomenology in each model is presented in Sect. 6. Lastly, we summarize the results and make conclusion in Sect. 7.

2 $U(1)_X$ anomaly cancellation

As stated, we extend the SM by adding an extra $U(1)_X$ gauge symmetry, such as

$$SU(3)_C \otimes SU(2)_L \otimes U(1)_Y \otimes U(1)_X. \tag{1}$$

The new charge, labeled as X, combines lepton and baryon numbers,

$$X = xB + yL, \tag{2}$$

and depends on family. That said, when X acts on a flavor i, it becomes $X_i = x_i B + y_i L$, where x_i and y_i are functions of i for $i = 1, 2, \ldots, N_f$, while B (L) denotes total baryon (lepton) number. The standard model fermions transform under the gauge symmetry (1) as

$$l_{iL} = (\nu_{iL}, e_{iL})^T \sim (\mathbf{1}, \mathbf{2}, -1/2, y_i), \tag{3}$$
$$e_{iR} \sim (\mathbf{1}, \mathbf{1}, -1, y_i), \tag{4}$$
$$q_{iL} = (u_{iL}, d_{iL})^T \sim (\mathbf{3}, \mathbf{2}, 1/6, x_i/3), \tag{5}$$
$$u_{iR} \sim (\mathbf{3}, \mathbf{1}, 2/3, x_i/3), \quad d_{iR} \sim (\mathbf{3}, \mathbf{1}, -1/3, x_i/3). \tag{6}$$

First, the anomaly $[SU(2)_L]^2 U(1)_X \sim \sum_{\text{doublets}} X_{f_L}$ vanishes if $\sum_i (x_i + y_i) = 0$. This equation contains $2N_f$ unknowns because of $i = 1, 2, \ldots, N_f$ and has an infinite number of solutions. Different solutions can be derived by imposing some suitable assumptions, which would lead to distinct kinds of new physics. For example, the $U(1)_{B-L}$ model with $x_i = -y_i = 1$ universally for every i makes the anomaly vanishing within each family similar to the SM, and in this case, both the $U(1)_{B-L}$ model and the SM cannot explain the existence of just three fermion families. As the perspective of this work, we assume that only x_i parameters depend on family, whereas y_i parameters do not, i.e. $y_i = z$

for every i, where z is arbitrarily nonzero. Additionally, the x_i parameters relate to the y_i parameters via the color number 3, namely, $x_{1,2,\ldots,n} = -3z$ and $x_{n+1,n+2,\ldots,n+m} = 3z$, where $n + m = N_f$. Hence, the anomaly cancellation becomes $3[n(-z) + mz] + N_f z = 0$, or equivalently

$$N_f = 3(n - m). \tag{7}$$

Since n and m are integer numbers, Eq. (7) implies the number of fermion families to be a multiple of the color number, 3. On the other hand, the QCD asymptotic freedom condition requires the family number to be less than or equal to 8, thus $N_f = 3$ and 6. The realistic solution is $N_f = 3$ as coinciding with experiment [4], which implies $n = 2$ and $m = 1$. For convenience in reading, we use two kinds of fermion family indices, $a, b = 1, 2, 3$ according to $N_f = 3$ and $\alpha, \beta = 1, 2$ according to $n = 2$, hereafter.

With the fermion content as in Eqs. (3)–(6), the $[\text{Gravity}]^2 U(1)_X$ and $[U(1)_X]^3$ anomalies are not canceled, which are given by

$$[\text{Gravity}]^2 U(1)_X \sim \sum_{\text{fermions}} (X_{f_L} - X_{f_R}) = 3z, \tag{8}$$

$$[U(1)_X]^3 \sim \sum_{\text{fermions}} (X_{f_L}^3 - X_{f_R}^3) = 3z^3. \tag{9}$$

Similar to the $U(1)_{B-L}$ extension, to cancel these anomalies, right-handed neutrinos that transform nontrivially under the gauge symmetry (1), i.e. $\nu_{iR} \sim (\mathbf{1}, \mathbf{1}, 0, X_{\nu_{iR}})$ for $X_{\nu_{iR}} \neq 0$, are necessarily introduced as fundamental fields, where $i = 1, 2, \ldots, N_R$ with N_R is the number of right-handed neutrinos added. Additionally, their $X_{\nu_{iR}}$ charges must satisfy

$$\sum_{i=1}^{N_R} X_{\nu_{iR}} = 3z, \qquad \sum_{i=1}^{N_R} X_{\nu_{iR}}^3 = 3z^3. \tag{10}$$

Solving the equations in (10), we obtain the following results: there is no solution when $N_R = 1$; there are only complex solutions when $N_R = 2$, which are unacceptable; and there is an infinite number of real solutions when $N_R \geq 3$. Note that the ν_R results obtained here include those in the $B - L$ extension corresponding to the case of $z = -1$. Particularly considering the case of $N_R = 3$ and requiring that at least two of three right-handed neutrinos be identical responsible for neutrino mass generation, we obtain two definite solutions. The first solution is $X_{\nu_{1,2,3R}} = z$, called conventional solution. The second solution is $X_{\nu_{1,2R}} = 4z$ and $X_{\nu_{3R}} = -5z$, called alternative solution. Each of these solutions implies a realistic model, which will be investigated in the subsequent sections of the present work.

Last, but not least, for the remaining non-trivial anomalies, the $[SU(3)_C]^2 U(1)_X$ anomaly is automatically canceled because the left and right chiral quarks have the same X value, and the anomalies $[U(1)_Y]^2 U(1)_X$ and $[U(1)_X]^2 U(1)_Y$ also

automatically vanish due to right-handed neutrinos having zero hypercharge.

3 Conventional $U(1)_X$ model

3.1 Particle content

In the conventional $U(1)_X$ model, three right-handed neutrinos are universal under $U(1)_X$. The fermion and scalar contents, as well as their quantum numbers under the gauge symmetry (1), are presented in Table 1, in which z is arbitrarily nonzero. In the scalar sector, besides the SM Higgs doublet labeled as Φ, a scalar singlet χ is necessarily presented to break $U(1)_X$, determining a residual symmetry Z_2, as well as generating appropriate right-handed neutrino masses through the coupling $\nu_R \nu_R \chi$. The scalar multiplets develop vacuum expectation values (VEVs),

$$\langle\Phi\rangle = \begin{pmatrix} 0 \\ \frac{v}{\sqrt{2}} \end{pmatrix}, \qquad \langle\chi\rangle = \frac{\Lambda}{\sqrt{2}}, \tag{11}$$

satisfying $\Lambda \gg v = 246$ GeV for consistency with the SM.

3.2 Matter parity and implication for single-component dark matter

With the assumption $\Lambda \gg v$, the gauge symmetry is broken as $SU(3)_C \otimes SU(2)_L \otimes U(1)_Y \otimes U(1)_X \xrightarrow{\Lambda} SU(3)_C \otimes SU(2)_L \otimes U(1)_Y \otimes R \xrightarrow{v} SU(3)_C \otimes U(1)_Q \otimes R$, where $Q = T_3 + Y$ is as usual, while R is a residual symmetry of $U(1)_X$ that conserves the χ vacuum. As being a $U(1)_X$ transformation, we have $R = e^{i\delta X}$, where δ is a transforming parameter. The vacuum conservation condition $R\langle\chi\rangle = \langle\chi\rangle$ implies $e^{i\delta(-2z)} = 1$, or equivalently $\delta = k\pi/z$ for k integer. Hence, the residual symmetry is

$$R = e^{ik\pi X/z} = (-1)^{kX/z}. \tag{12}$$

It is clear that if $k = 0$, then $R = 1$ for all fields and every z, which is the identity transformation. Additionally, for $k \neq 0$, the relevant transformation $R = 1$ is valid for all fields, given the minimal value of $|k| = 2$. Hence, the residual symmetry R is automorphic to a discrete group, such as $\mathcal{Z}_2 = \{1, g\}$ with $g = (-1)^{X/z}$ and $g^2 = 1$. Because the spin parity, $p_s = (-1)^{2s}$, is always conserved by the Lorentz symmetry, we conveniently multiply the discrete group with the spin parity group $S = \{1, p_s\}$ with $p_s^2 = 1$, to perform a new group $\mathcal{Z}_2 \otimes S$, which has an invariant discrete subgroup to be

$$Z_2 = \{1, p\} \tag{13}$$

with $p = g \times p_s = (-1)^{X/z+2s}$ and $p^2 = 1$. Therefore, we decompose $\mathcal{Z}_2 \otimes S \cong [(\mathcal{Z}_2 \otimes S)/Z_2] \otimes Z_2$. Since

$[(\mathcal{Z}_2 \otimes S)/Z_2] = \{\{1, p\}, \{g, p_s\}\}$ is conserved if Z_2 is conserved, we consider Z_2 to be a residual symmetry alternative to $\mathcal{Z}_2$. As usual, Z_2 has two one-dimensional irreducible representations, $\underline{1}$ according to $p = 1$ and $\underline{1}'$ according to $p = -1$. All the SM fields and new scalar singlet χ transform trivially under Z_2, indicated in the last column of Table 1.

That said, the conventional $U(1)_X$ model implies exactly a matter parity, Z_2. Because of the Z_2 conservation, the model can contain several scenarios for single-component dark matter, such as a single dark field to be either a dark (vectorlike) fermion, labeled ξ, or a dark scalar singlet, labeled η, which all transform nontrivially under Z_2, i.e., $p = -1$. In what follows, we extend the present model to include both ξ and η candidates. These fields and their simplest quantum numbers are collected to the last two rows of Table 1. Note that the candidate ξ is vectorlike, and thus does not contribute to any gauge anomalies, while the candidate η possesses vanishing VEV, i.e. $\langle\eta\rangle = 0$, due to the conservation of Z_2.

3.3 Fermion mass and seesaw mechanism

The spontaneous symmetry breaking will generate fermion masses through the Yukawa interactions, such as

$$\begin{aligned}
\mathcal{L} \supset{} & h_{ab}^e \bar{l}_{aL} \Phi e_{bR} + h_{ab}^\nu \bar{l}_{aL} \tilde{\Phi} \nu_{bR} + \frac{1}{2} f_{ab}^\nu \bar{\nu}_{aR}^c \nu_{bR} \chi \\
& + h_{\alpha\beta}^d \bar{q}_{\alpha L} \Phi d_{\beta R} + h_{\alpha\beta}^u \bar{q}_{\alpha L} \tilde{\Phi} u_{\beta R} \\
& + h_{33}^d \bar{q}_{3L} \Phi d_{3R} + h_{33}^u \bar{q}_{3L} \tilde{\Phi} u_{3R} \\
& + \frac{h_{\alpha 3}^d}{M} \bar{q}_{\alpha L} \Phi \chi d_{3R} + \frac{h_{3\alpha}^u}{M} \bar{q}_{3L} \tilde{\Phi} \chi^* u_{\alpha R} \\
& + \frac{h_{3\alpha}^d}{M} \bar{q}_{3L} \Phi \chi^* d_{\alpha R} + \frac{h_{\alpha 3}^u}{M} \bar{q}_{\alpha L} \tilde{\Phi} \chi u_{3R} \\
& + y_a \bar{\xi}_L \eta \nu_{aR} - m_\xi \bar{\xi}_L \xi_R + \text{H.c.}, \tag{14}
\end{aligned}$$

where we have labeled $\tilde{\Phi} = i\sigma_2 \Phi^*$ with σ_2 to be the second Pauli matrix, and M is a new physics (or cutoff) scale that defines the effective interactions. Note that the couplings h, f^ν, and y are dimensionless, whereas m_ξ has a mass dimension.

From the above interactions, we obtain mass matrices for charged leptons, down-type quarks, and up-type quarks, which are given by

$$[M_e]_{ab} = -h_{ab}^e \frac{v}{\sqrt{2}}, \tag{15}$$

$$[M_d]_{\alpha\beta} = -h_{\alpha\beta}^d \frac{v}{\sqrt{2}}, \qquad [M_d]_{33} = -h_{33}^d \frac{v}{\sqrt{2}}, \tag{16}$$

$$[M_d]_{\alpha 3} = -h_{\alpha 3}^d \frac{v\Lambda}{2M}, \qquad [M_d]_{3\beta} = -h_{3\beta}^d \frac{v\Lambda}{2M}, \tag{17}$$

$$[M_u]_{\alpha\beta} = -h_{\alpha\beta}^u \frac{v}{\sqrt{2}}, \qquad [M_u]_{33} = -h_{33}^u \frac{v}{\sqrt{2}}, \tag{18}$$

$$[M_u]_{\alpha 3} = -h_{\alpha 3}^u \frac{v\Lambda}{2M}, \qquad [M_u]_{3\beta} = -h_{3\beta}^u \frac{v\Lambda}{2M}. \tag{19}$$

Table 1 Matter content in the conventional $U(1)_X$ model

Multiplets	$SU(3)_C$	$SU(2)_L$	$U(1)_Y$	$U(1)_X$	Z_2
$l_{aL} = (\nu_{aL}, e_{aL})^T$	**1**	**2**	$-\frac{1}{2}$	z	$+$
ν_{aR}	**1**	**1**	0	z	$+$
e_{aR}	**1**	**1**	-1	z	$+$
$q_{\alpha L} = (u_{\alpha L}, d_{\alpha L})^T$	**3**	**2**	$\frac{1}{6}$	$-z$	$+$
$u_{\alpha R}$	**3**	**1**	$\frac{2}{3}$	$-z$	$+$
$d_{\alpha R}$	**3**	**1**	$-\frac{1}{3}$	$-z$	$+$
$q_{3L} = (u_{3L}, d_{3L})^T$	**3**	**2**	$\frac{1}{6}$	z	$+$
u_{3R}	**3**	**1**	$\frac{2}{3}$	z	$+$
d_{3R}	**3**	**1**	$-\frac{1}{3}$	z	$+$
$\Phi = (\Phi_1^+, \Phi_2^0)^T$	**1**	**2**	$\frac{1}{2}$	0	$+$
χ	**1**	**1**	0	$-2z$	$+$
ξ	**1**	**1**	0	$2z$	$-$
η	**1**	**1**	0	z	$-$

Therefore, the small mixing between the third quark family and the first two quark families can be understood by either $h_{\alpha 3}, h_{3\beta} < h_{\alpha \beta}, h_{33}$ or $\Lambda < M$. Diagonalizing these mass matrices, we get the masses of the relevant particles and the Cabibbo–Kobayashi–Maskawa matrix, as expected.

Concerning neutrinos, $\nu_{aL,R}$ achieve a Dirac mass via h^ν coupling, $[M_D]_{ab} = -h_{ab}^\nu \frac{v}{\sqrt{2}}$, while ν_{aR} obtains a Majorana mass via f^ν coupling, $[M_M]_{ab} = -f_{ab}^\nu \frac{\Lambda}{\sqrt{2}}$. Thus, the total mass matrix of neutrinos takes the form,

$$\mathcal{L}_{\text{Yukawa}} \supset -\frac{1}{2}(\bar{\nu}_L, \bar{\nu}_R^c) \begin{pmatrix} 0 & M_D \\ M_D^T & M_M \end{pmatrix} \begin{pmatrix} \nu_L^c \\ \nu_R \end{pmatrix} + \text{H.c.} \quad (20)$$

Because of $\Lambda \gg v$, i.e. $M_M \gg M_D$, the active neutrinos $\sim \nu_L$ acquire a small mass via the canonical seesaw to be

$$[m_\nu]_{ab} = -[M_D M_M^{-1} M_D^T]_{ab} = (h^\nu)^2 (f^\nu)^{-1} v^2 / \sqrt{2}\Lambda, \quad (21)$$

whereas the heavy neutrinos $\sim \nu_R$ obtain a large mass at the new physics scale Λ. Additionally, if h^ν is very small, $h^\nu \sim 10^{-5}$, similar to electron Yukawa coupling, while fixing $f^\nu \sim 0.6$, the observed value $m_\nu \sim 0.1$ eV requires $\Lambda \sim 15$ TeV. Alternatively, given that $(h^\nu)^2/f^\nu \sim 1$, the model predicts $\Lambda \sim 10^{14}$ TeV close to the grand unification scale.

Lastly, since the VEV of dark scalar singlet vanishes due to Z_2 conservation, the dark fermion does not mix with right-handed neutrinos despite the term $y_a \bar{\xi}_L \eta \nu_{aR}$. Therefore, the dark fermion ξ is a physical field by itself, with an arbitrary mass, m_ξ.

3.4 Gauge sector

When the gauge symmetry breaking takes place, the gauge bosons acquire masses via the kinetic terms of scalar fields, $\sum_S (D^\mu S)^\dagger (D_\mu S)$, where S runs over scalar multiplets. The covariant derivative is defined as

$$D_\mu = \partial_\mu + ig_s t_p G_{p\mu} + ig T_j A_{j\mu} + ig_Y Y B_\mu + ig_X X C_\mu, \quad (22)$$

in which (g_s, g, g_Y, g_X), (t_p, T_j, Y, X), and $(G_{p\mu}, A_{j\mu}, B_\mu, C_\mu)$ denote coupling constants, generators, and gauge bosons of $(SU(3)_C, SU(2)_L, U(1)_Y, U(1)_X)$ groups, respectively.

The charged gauge bosons, $W^\pm$, take the form with corresponding mass,

$$W^\pm = \frac{1}{\sqrt{2}}(A_1 \mp i A_2), \quad m_W = \frac{g^2 v^2}{4}, \quad (23)$$

which implies $v = 246$ GeV. Because the SM scalar doublet Φ is not charged under $U(1)_X$, while the new scalar singlet χ is not charged under the SM gauge group, there is no mass mixing between the SM neutral gauge boson Z and the new gauge boson Z' coming from gauge symmetry breaking.[1] It is straightforward to define the photon field A, the SM neutral gauge boson Z, and the new neutral gauge boson Z', with their corresponding masses, as

$$A = s_W A_3 + c_W B, \quad m_A = 0, \quad (24)$$

$$Z = c_W A_3 - s_W B, \quad m_Z^2 = \frac{g^2 v^2}{4c_W^2}, \quad (25)$$

$$Z' = C, \quad m_{Z'}^2 = 4g_X^2 z^2 \Lambda^2, \quad (26)$$

where the Weinberg's angle is defined by $t_W \equiv \tan(\theta_W) = g_Y/g$, as usual.

---

[1] Kinetic mixing term between the two $U(1)$ gauge fields if imposed would cause a small effect, as suppressed.

3.5 Scalar sector

In presence of two scalar singlets χ and η as well as the SM scalar doublet Φ, the total scalar potential is given by

$$V = \mu_1^2 \Phi^\dagger \Phi + \mu_2^2 \chi^* \chi + \mu_3^2 \eta^* \eta + \lambda_1 (\Phi^\dagger \Phi)^2 + \lambda_2 (\chi^* \chi)^2$$
$$+ \lambda_3 (\eta^* \eta)^2 + \lambda_4 (\Phi^\dagger \Phi)(\chi^* \chi)$$
$$+ \lambda_5 (\Phi^\dagger \Phi)(\eta^* \eta) + \lambda_6 (\chi^* \chi)(\eta^* \eta), \quad (27)$$

where λ's is dimensionless, whereas μ's has a mass dimension. Necessary conditions for this potential to be bounded from below as well as to yield desirable vacuum structure are

$$\lambda_{1,2,3} > 0, \quad \mu_{1,2}^2 < 0, \quad \mu_3^2 > 0, \quad |\mu_1| \ll |\mu_2|. \quad (28)$$

To obtain the potential minimum and physical scalar spectrum, we expand

$$\Phi = \begin{pmatrix} \Phi_1^+ \\ \frac{1}{\sqrt{2}}(v + S_1 + i A_1) \end{pmatrix}, \quad (29)$$

$$\chi = \frac{1}{\sqrt{2}}(\Lambda + S_2 + i A_2), \quad \eta = \frac{1}{\sqrt{2}}(S_3 + i A_3). \quad (30)$$

Substituting them to the scalar potential (27), we get the potential minimum conditions,

$$\Lambda^2 = \frac{2(\lambda_4 \mu_1^2 - 2\lambda_1 \mu_2^2)}{4\lambda_1 \lambda_2 - \lambda_4^2}, \quad v^2 = \frac{2(\lambda_4 \mu_2^2 - 2\lambda_2 \mu_1^2)}{4\lambda_1 \lambda_2 - \lambda_4^2}. \quad (31)$$

Further, we obtain physical scalar fields, such as

$$\Phi \simeq \begin{pmatrix} G_W^+ \\ \frac{1}{\sqrt{2}}(v + H + i G_Z) \end{pmatrix},$$
$$\chi \simeq \frac{1}{\sqrt{2}}(\Lambda + H' + i G_{Z'}), \quad (32)$$

where the mixing between two CP-even scalars $H = S_1$ and $H' = S_2$ is suppressed by v/Λ, which has been neglected for simplicity. That said, H is identical to the SM Higgs boson, while H' is a new Higgs boson associated with $U(1)_X$ breaking. Their masses are

$$m_H^2 \simeq 2\lambda_1 v^2, \quad m_{H'}^2 \simeq 2\lambda_2 \Lambda^2. \quad (33)$$

The CP-odd fields G_W, G_Z, and $G_{Z'}$ are massless Goldstone bosons, which are absorbed by W, Z, and Z' gauge bosons, respectively.

The dark scalars S_3 and A_3 do not mix with the other scalars, because of the Z_2 conservation, and they are degenerate in mass. Therefore, they define a physical complex field η with an arbitrary mass to be

$$m_\eta^2 = \mu_3^2 + \frac{1}{2}\lambda_5 v^2 + \frac{1}{2}\lambda_6 \Lambda^2. \quad (34)$$

4 Alternative $U(1)_X$ model

We would like to remind the reader that this model and the previous model share many common notations, which have similar properties and should be understood.

4.1 Particle content

In the alternative $U(1)_X$ model, only two right-handed neutrinos are universal under $U(1)_X$, which is different from the previous model. The particle content and their quantum numbers under the gauge symmetry in (1) are presented in Table 2. Concerning the scalar sector, in addition to the SM scalar doublet Φ, the two scalar singlets $\chi_{1,2}$ are necessarily included to break $U(1)_X$, determining a residual symmetry Z_2 as well as generating appropriate Majorana masses for right-handed neutrinos through couplings $\nu_{\alpha R}\nu_{\alpha R}\chi_1$ and $\nu_{3R}\nu_{3R}\chi_2$. The scalar multiplets develop VEVs, such as

$$\langle \Phi \rangle = \begin{pmatrix} 0 \\ \frac{v}{\sqrt{2}} \end{pmatrix}, \quad \langle \chi_1 \rangle = \frac{\Lambda_1}{\sqrt{2}}, \quad \langle \chi_2 \rangle = \frac{\Lambda_2}{\sqrt{2}}, \quad (35)$$

satisfying $\Lambda_{1,2} \gg v = 246$ GeV for consistency with the SM.

It is stressed that since the charge assignment of $U(1)_X$, the neutrino mass is forbidden at tree level. We thus introduce two more scalars, namely, a doublet ϕ linking l_{aL} to $\nu_{\alpha R}$ and a singlet η linking ϕ to $\Phi \chi_1$ as well as to χ_2. It is noted that both ϕ and η are odd under a residual gauge symmetry Z_2 of $U(1)_X$ (see below) and cannot develop VEV due to the conservation of this Z_2. This implements a scotogenic mechanism for generating appropriate neutrino masses, as shown in Fig. 1 [29].

4.2 Matter parity and implication for two-component dark matter

The spontaneous symmetry breaking of the gauge symmetry (1) down to $SU(3)_C \otimes SU(2)_L \otimes U(1)_Y \otimes R$ is implemented by the new scalar singlets, $\chi_{1,2}$. Then, the SM gauge group is spontaneously broken to the low energy theory by the SM Higgs doublet, Φ, as usual. Because R is a residual symmetry of $U(1)_X$ that conserves both the vacua of χ_1 and χ_2, the transformation $R = e^{i\delta X}$ satisfies simultaneously $R\langle \chi_{1,2} \rangle = \langle \chi_{1,2} \rangle$, where δ is a transforming parameter. This leads to $e^{i\delta(-8z)} = 1$ and $e^{i\delta(10z)} = 1$, implying $\delta = k\pi/z$ for k integer, thus $R = e^{ik\pi X/z} = (-1)^{kX/z}$. Similar to the previous model, the residual symmetry R is automorphic to the discrete group $\mathcal{Z}_2 = \{1, g\}$ with $g = (-1)^{X/z}$ and $g^2 = 1$. Also, since the spin parity $p_s = (-1)^{2s}$ is always conserved, we multiply p_s with g to form $p = g \times p_s = (-1)^{X/z+2s}$, which performs a discrete group $Z_2 = \{1, p\}$ with $p^2 = 1$ to be a residual symmetry instead of $\mathcal{Z}_2$, for convenience.

Table 2 Matter content in the alternative $U(1)_X$ model

Multiplets	$SU(3)_C$	$SU(2)_L$	$U(1)_Y$	$U(1)_X$	Z_2
$l_{aL} = (\nu_{aL}, e_{aL})^T$	**1**	**2**	$-\frac{1}{2}$	z	$+$
$\nu_{\alpha R}$	**1**	**1**	0	$4z$	$-$
ν_{3R}	**1**	**1**	0	$-5z$	$+$
e_{aR}	**1**	**1**	-1	z	$+$
$q_{\alpha L} = (u_{\alpha L}, d_{\alpha L})^T$	**3**	**2**	$\frac{1}{6}$	$-z$	$+$
$u_{\alpha R}$	**3**	**1**	$\frac{2}{3}$	$-z$	$+$
$d_{\alpha R}$	**3**	**1**	$-\frac{1}{3}$	$-z$	$+$
$q_{3L} = (u_{3L}, d_{3L})^T$	**3**	**2**	$\frac{1}{6}$	z	$+$
u_{3R}	**3**	**1**	$\frac{2}{3}$	z	$+$
d_{3R}	**3**	**1**	$-\frac{1}{3}$	z	$+$
$\Phi = (\Phi_1^+, \Phi_2^0)^T$	**1**	**2**	$\frac{1}{2}$	0	$+$
χ_1	**1**	**1**	0	$-8z$	$+$
χ_2	**1**	**1**	0	$10z$	$+$
$\phi = (\phi_1^0, \phi_2^-)^T$	**1**	**2**	$-\frac{1}{2}$	$-3z$	$-$
η	**1**	**1**	0	$-5z$	$-$

Under Z_2, all the SM fields, ν_{3R}, and $\chi_{1,2}$ are even, whereas $\nu_{\alpha R}$, ϕ, and η are all odd, as presented in the last column of Table 2.

The model under consideration is of particular interest, with a novel implication for two-component dark matter. Indeed, because of the conservation of Z_2, the lightest field of odd fields $\nu_{\alpha R}$, ϕ, η is stabilized, impossibly decayed to normal fields, providing a dark matter candidate. In addition, the third right-handed neutrino ν_{3R} with charge $X = -5z$ do not couple to any SM particles due to the gauge invariance and hence it reveals accidentally an alternative candidate for dark matter. In other words, a promising scenario for two-component dark matter, which consists of the lightest odd-field and ν_{3R}, is hinted.

4.3 Gauge sector

In the current model, since the SM scalar doublet Φ does not transform under $U(1)_X$ and that the new scalar singlets $\chi_{1,2}$ do not transform under $SU(2)_L \otimes U(1)_Y$, there is no tree-level mixing between the gauge bosons Z and Z', similar to the previous model. The SM gauge bosons $W^\pm$, A, Z and new gauge boson Z' with their masses are given by

$$W^\pm = \frac{1}{\sqrt{2}}(A_1 \mp i A_2), \quad m_W^2 = \frac{g^2 v^2}{4}, \tag{36}$$

$$A = s_W A_3 + c_W B, \quad m_A = 0, \tag{37}$$

$$Z = c_W A_3 - s_W B, \quad m_Z^2 = \frac{g^2 v^2}{4 c_W^2}, \tag{38}$$

$$Z' = C, \quad m_{Z'}^2 = g_X^2 z^2 (64\Lambda_1^2 + 100\Lambda_2^2), \tag{39}$$

where the Weinberg's angle is defined by $t_W = g_Y/g$, as usual.

4.4 Scalar sector relevant for symmetry breaking

As shown above, two new scalar singlets $\chi_{1,2}$ break $U(1)_X$ to Z_2, and then the SM scalar doublet Φ breaks the $SU(2)_L \otimes U(1)_Y$ electroweak symmetry down to $U(1)_Q$, as usual. The scalar potential consisting of Φ, $\chi_{1,2}$ is given by

$$
\begin{aligned}
V \supset\ & \mu_0^2 \Phi^\dagger \Phi + \mu_1^2 \chi_1^* \chi_1 + \mu_2^2 \chi_2^* \chi_2 + \lambda_0 (\Phi^\dagger \Phi)^2 \\
& + \lambda_1 (\chi_1^* \chi_1)^2 + \lambda_2 (\chi_2^* \chi_2)^2 + (\Phi^\dagger \Phi)[\lambda_3(\chi_1^* \chi_1) \\
& + \lambda_4 (\chi_2^* \chi_2)] + \lambda_5 (\chi_1^* \chi_1)(\chi_2^* \chi_2).
\end{aligned} \tag{40}
$$

The necessary conditions for this potential to be bounded from below as well as yielding a desirable vacuum structure are

$$\lambda_{0,1,2} > 0, \quad \mu_{0,1,2}^2 < 0, \quad |\mu_0| \ll |\mu_{1,2}|. \tag{41}$$

Note that the scalar potential in Eq. (40) actually has a global $U(1)$ symmetry in addition to the gauge symmetry. Consequently, there is a physical Goldstone boson in the particle spectrum after the spontaneous symmetry breaking, which was discussed in [30].

Expanding the scalar fields around their VEVs as

$$\Phi = \begin{pmatrix} \Phi_1^+ \\ \frac{1}{\sqrt{2}}(v + S_1 + i A_1) \end{pmatrix}, \tag{42}$$

$$\chi_1 = \frac{1}{\sqrt{2}}(\Lambda_1 + S_2 + i A_2), \quad \chi_2 = \frac{1}{\sqrt{2}}(\Lambda_2 + S_3 + i A_3), \tag{43}$$

and substituting these expressions into the scalar potential (40), we obtain the following potential minimum conditions:

$$2\mu_0^2 + 2\lambda_0 v^2 + \lambda_3 \Lambda_1^2 + \lambda_4 \Lambda_2^2 = 0, \tag{44}$$

$$2\mu_1^2 + \lambda_3 v^2 + 2\lambda_1 \Lambda_1^2 + \lambda_5 \Lambda_2^2 = 0, \tag{45}$$

$$2\mu_2^2 + \lambda_4 v^2 + \lambda_5 \Lambda_1^2 + 2\lambda_2 \Lambda_2^2 = 0. \tag{46}$$

Further, we obtain physical scalar fields, such as

$$\Phi \simeq \begin{pmatrix} G_W^+ \\ \frac{1}{\sqrt{2}}(v + H + iG_Z) \end{pmatrix}, \tag{47}$$

$$\chi_1 \simeq \frac{1}{\sqrt{2}}(\Lambda_1 + H_1 + i\mathcal{A}),$$

$$\chi_2 \simeq \frac{1}{\sqrt{2}}(\Lambda_2 + H_2 + iG_{Z'}), \tag{48}$$

where we have assumed $\Lambda_2 \gg \Lambda_1 \gg v$ and neglected the mixing among three CP-even scalars for simplicity. That said, the assumption $\Lambda_2 \gg \Lambda_1$ would lead to an attractive scenario of two-component fermion dark matter (cf. Sect. 6.2 below). Above, H is identical to the SM Higgs boson, whereas $H_{1,2}$ are the new Higgs bosons. Their masses are approximately given by

$$m_H^2 \simeq 2\lambda_0 v^2, \quad m_{H_1}^2 \simeq 2\lambda_1 \Lambda_1^2, \quad m_{H_2}^2 \simeq 2\lambda_2 \Lambda_2^2. \tag{49}$$

Additionally, G_W, G_Z, and $G_{Z'}$ are the massless Goldstone bosons absorbed by W, Z, and Z' gauge bosons, respectively, whereas $\mathcal{A}$ is a physical Goldstone boson as predicted.

The presence of a physical Goldstone boson, in principle, poses some issues for the model. However, the physical Goldstone boson $\mathcal{A}$ here is probably safe because it does not directly couple to the SM particles except for the Higgs boson whose couplings are well controlled by the parameters in the potential, and it decouples from the thermal bath in the early universe. Indeed, the $\lambda_3(\Phi^\dagger\Phi)(\chi_1^*\chi_1)$ term allows the SM Higgs to decay into a pair of Goldstone bosons, inducing a tree-level contribution to partial width as $\Gamma_{H\to\mathcal{A}\mathcal{A}} \sim \lambda_3^2 v^2/32\pi m_H$. Taking $m_H \simeq 125.25$ GeV, the full width of the Higgs boson to be 3.2 MeV, and the branching ratio for invisible decay models must be less than 13% [4], we obtain a constraint on the coupling to be $|\lambda_3| \lesssim 0.009$. On the other hand, following the discussion in Ref. [31], since the $H_{1,2}$ and Z' bosons that couple to $\mathcal{A}$ are heavy, their interactions with $\mathcal{A}$ decouple at sufficiently high temperature in the early universe. Concerning the interaction between $\mathcal{A}$ and the SM fermions, the ratio R between the rate of collisions of $\mathcal{A}$ with fermion f and the expansion rate of the universe, at a temperature T, is roughly given by $R \sim \lambda_3^2 m_f^2 (kT)^5 m_P/(m_{H_1} m_H)^4$ [31], where m_f is the mass of the fermion f, m_P is the Planck mass, and k is the Boltzmann constant. The decoupling of $\mathcal{A}$ from thermal equilibrium occurs when the ratio is equal to unity, i.e. $R \sim 1$. Taking $m_P \simeq 1.22 \times 10^{19}$ GeV [4], and

assuming $m_f = m_\tau = 1.77686$ GeV (the tauon mass), we obtain a decoupling temperature as $T_d \sim 9.54$ GeV, which is consistent with the condition $T > m_\tau$, given that $k \sim 1$, $|\lambda_3| \sim 0.009$, and $m_{H_1} = 1$ TeV. In addition, it is clear that this decoupling temperature is far above the neutrino decoupling temperature approximately a few MeV, as well as the QCD phase transition temperature about 200 MeV. Therefore, the contribution of $\mathcal{A}$ to the density of radiation in the Universe that is usually parametrized by the effective neutrino number N_{eff} is given by

$$\Delta N_{\text{eff}} = \frac{4}{7}\left(\frac{h_\gamma^{\text{BBN}}}{h_\gamma^{\text{dec}}}\right)^{4/3} \lesssim \frac{4}{7}\left(\frac{10.75}{60}\right)^{4/3} \simeq 0.06, \tag{50}$$

where h_γ^{BBN} and h_γ^{dec} are the entropy degrees of freedom of the plasma at the time of big bang nucleosynthesis and of the $\mathcal{A}$ decoupling, respectively. This result is in agreement with the current bound on N_{eff}, i.e. $N_{\text{eff}} = 2.99 \pm 0.17$ [1]. All imply that if $|\lambda_3| \lesssim 0.009$, $\mathcal{A}$ decouples from the thermal bath in the early universe around $\mathcal{O}(1)$ GeV temperature, and this does not cause serious problems in particle physics or cosmology.

4.5 Fermion mass and scotogenic mechanism

When the scalar multiplets develop VEVs, the fermions acquire masses through Yukawa interactions, such as

$$\begin{aligned} \mathcal{L} \supset &\, h_{ab}^e \bar{l}_{aL} \Phi e_{bR} + h_{\alpha\beta}^d \bar{q}_{\alpha L} \Phi d_{\beta R} + h_{\alpha\beta}^u \bar{q}_{\alpha L} \tilde{\Phi} u_{\beta R} \\ &+ h_{33}^d \bar{q}_{3L} \Phi d_{3R} + h_{33}^u \bar{q}_{3L} \tilde{\Phi} u_{3R} \\ &+ \frac{h_{\alpha 3}^d}{M^2} \bar{q}_{\alpha L} \Phi \chi_1^* \chi_2^* d_{3R} + \frac{h_{3\beta}^u}{M^2} \bar{q}_{3L} \tilde{\Phi} \chi_1 \chi_2 u_{\beta R} \\ &+ \frac{h_{3\beta}^d}{M^2} \bar{q}_{3L} \Phi \chi_1 \chi_2 d_{\beta R} + \frac{h_{\alpha 3}^u}{M^2} \bar{q}_{\alpha L} \tilde{\Phi} \chi_1^* \chi_2^* u_{3R} \\ &+ h_{\alpha\beta}^\nu \bar{l}_{aL} \phi \nu_{\beta R} + \frac{1}{2} f_{\alpha\beta}^\nu \bar{\nu}_{\alpha R}^c \nu_{\beta R} \chi_1 \\ &+ \frac{1}{2} f_{33}^\nu \bar{\nu}_{3R}^c \nu_{3R} \chi_2 + \text{H.c.} \end{aligned} \tag{51}$$

The right-handed neutrinos capture large Majorana masses at $\Lambda_{1,2}$ scales,

$$m_{\nu_{1R}} = -f_{11}^\nu \frac{\Lambda_1}{\sqrt{2}}, \quad m_{\nu_{2R}} = -f_{22}^\nu \frac{\Lambda_1}{\sqrt{2}},$$

$$m_{\nu_{3R}} = -f_{33}^\nu \frac{\Lambda_2}{\sqrt{2}}, \tag{52}$$

assuming that $f_{\alpha\beta}^\nu$ is flavor diagonal, without loss of generality, i.e. $\nu_{1,2,3R}$ are physical fields by themselves. Whereas, the charged leptons, down-type quarks, and up-type quarks obtain mass matrices at the weak scale, namely

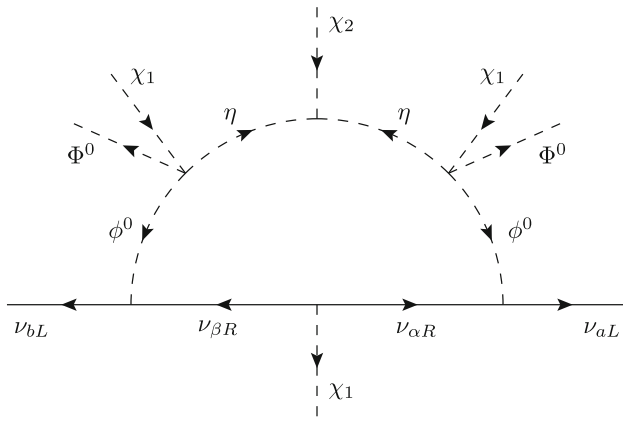$$[M_e]_{ab} = -h_{ab}^e \frac{v}{\sqrt{2}}, \tag{53}$$

Fig. 1 Radiative generation of neutrino mass through dark matter

$$[M_d]_{\alpha\beta} = -h_{\alpha\beta}^d \frac{v}{\sqrt{2}}, \qquad [M_d]_{33} = -h_{33}^d \frac{v}{\sqrt{2}}, \qquad (54)$$

$$[M_d]_{\alpha 3} = -h_{\alpha 3}^d \frac{v\Lambda_1\Lambda_2}{2\sqrt{2}M^2}, \qquad [M_d]_{3\beta} = -h_{3\beta}^d \frac{v\Lambda_1\Lambda_2}{2\sqrt{2}M^2}, \qquad (55)$$

$$[M_u]_{\alpha\beta} = -h_{\alpha\beta}^u \frac{v}{\sqrt{2}}, \qquad [M_u]_{33} = -h_{33}^u \frac{v}{\sqrt{2}}, \qquad (56)$$

$$[M_u]_{\alpha 3} = -h_{\alpha 3}^u \frac{v\Lambda_1\Lambda_2}{2\sqrt{2}M^2}, \qquad [M_u]_{3\beta} = -h_{3\beta}^u \frac{v\Lambda_1\Lambda_2}{2\sqrt{2}M^2}. \qquad (57)$$

These mass matrices provide appropriate masses for the corresponding particles after diagonalization, given that $h_{\alpha 3}, h_{3\beta} < h_{\alpha\beta}, h_{33}$ and/or $\Lambda_{1,2} < M$.

Differing from the previous model, the active neutrinos in the current model obtain radiative Majorana masses through the scotogenic mechanism with the Z_2-odd fields $\nu_{\alpha R}, \phi$, and η, as described in Fig. 1. To get the relevant physical scalars, we consider the scalar potential related to ϕ and η, which is given by

$$\begin{aligned} V \supset{}& \mu_3^2 \phi^\dagger\phi + \mu_4^2 \eta^*\eta + \lambda_6(\phi^\dagger\phi)^2 + \lambda_7(\eta^*\eta)^2 \\ &+ (\Phi^\dagger\Phi)[\lambda_8(\phi^\dagger\phi) + \lambda_9(\eta^*\eta)] \\ &+ (\chi_1^*\chi_1)[\lambda_{10}(\phi^\dagger\phi) + \lambda_{11}(\eta^*\eta)] + (\chi_2^*\chi_2)[\lambda_{12}(\phi^\dagger\phi) \\ &+ \lambda_{13}(\eta^*\eta)] + \lambda_{14}(\phi^\dagger\phi)(\eta^*\eta) \\ &+ \lambda_{15}(\Phi^\dagger\phi)(\phi^\dagger\Phi) + \mu(\chi_2\eta\eta + \text{H.c.}) \\ &+ \lambda(\Phi\phi\eta\chi_1^* + \text{H.c.}). \end{aligned} \qquad (58)$$

The necessary conditions for this potential to be bounded from below as well as yielding the trivial vacua for both ϕ and η ensuring the Z_2 symmetry are $\mu_{3,4}^2 > 0$ and $\lambda_{6,7} > 0$. Expanding $\phi = ((S_4 + iA_4)/\sqrt{2}, \phi_2^-)^T$ and $\eta = (S_5 + iA_5)/\sqrt{2}$, then substituting them into the scalar potential, we obtain

$$V \supset \frac{1}{2}\begin{pmatrix} S_4 & S_5 \end{pmatrix} \begin{pmatrix} M_1^2 & -\frac{1}{2}\lambda v\Lambda_1 \\ -\frac{1}{2}\lambda v\Lambda_1 & M_2^2 + \sqrt{2}\mu\Lambda_2 \end{pmatrix} \begin{pmatrix} S_4 \\ S_5 \end{pmatrix}$$

$$+ \frac{1}{2}\begin{pmatrix} A_4 & A_5 \end{pmatrix} \begin{pmatrix} M_1^2 & \frac{1}{2}\lambda v\Lambda_1 \\ \frac{1}{2}\lambda v\Lambda_1 & M_2^2 - \sqrt{2}\mu\Lambda_2 \end{pmatrix} \begin{pmatrix} A_4 \\ A_5 \end{pmatrix}, \qquad (59)$$

where $M_1^2 = (2\mu_3^2 + \lambda_{10}\Lambda_1^2 + \lambda_{12}\Lambda_2^2 + \lambda_8 v^2)/2$ and $M_2^2 = (2\mu_4^2 + \lambda_{11}\Lambda_1^2 + \lambda_{13}\Lambda_2^2 + \lambda_9 v^2)/2$. Defining two mixing angles $\theta_{R,I}$ via the tan functions as

$$t_{2\theta_R} = \frac{\lambda v\Lambda_1}{M_1^2 - M_2^2 - \sqrt{2}\mu\Lambda_2},$$

$$t_{2\theta_I} = \frac{\lambda v\Lambda_1}{M_2^2 - M_1^2 - \sqrt{2}\mu\Lambda_2}, \qquad (60)$$

we get the physical fields

$$\mathcal{S}_1 = c_{\theta_R}S_4 - s_{\theta_R}S_5, \qquad \mathcal{S}_2 = s_{\theta_R}S_4 + c_{\theta_R}S_5, \qquad (61)$$

$$\mathcal{A}_1 = c_{\theta_I}A_4 - s_{\theta_I}A_5, \qquad \mathcal{A}_2 = s_{\theta_I}A_4 + c_{\theta_I}A_5, \qquad (62)$$

with respective masses,

$$m_{\mathcal{S}_1}^2 \simeq M_1^2 - \frac{\frac{1}{4}\lambda^2 v^2\Lambda_1^2}{M_2^2 - M_1^2 + \sqrt{2}\mu\Lambda_2},$$

$$m_{\mathcal{S}_2}^2 \simeq M_2^2 + \sqrt{2}\mu\Lambda_2 + \frac{\frac{1}{4}\lambda^2 v^2\Lambda_1^2}{M_2^2 - M_1^2 + \sqrt{2}\mu\Lambda_2}, \qquad (63)$$

$$m_{\mathcal{A}_1}^2 \simeq M_1^2 - \frac{\frac{1}{4}\lambda^2 v^2\Lambda_1^2}{M_2^2 - M_1^2 - \sqrt{2}\mu\Lambda_2},$$

$$m_{\mathcal{A}_2}^2 \simeq M_2^2 - \sqrt{2}\mu\Lambda_2 + \frac{\frac{1}{4}\lambda^2 v^2\Lambda_1^2}{M_2^2 - M_1^2 - \sqrt{2}\mu\Lambda_2}, \qquad (64)$$

in which the approximations come from the conditions $\Lambda_{1,2} \gg v$. Lastly, the radiative neutrino mass matrix is given by [32]

$$\begin{aligned} (m_\nu)_{ab} ={}& \frac{h_{a\alpha}^\nu h_{b\alpha}^\nu m_{\nu_{\alpha R}}}{32\pi^2} \left(\frac{c_{\theta_R}^2 m_{\mathcal{S}_1}^2}{m_{\mathcal{S}_1}^2 - m_{\nu_{\alpha R}}^2} \ln\frac{m_{\mathcal{S}_1}^2}{m_{\nu_{\alpha R}}^2} \right. \\ &- \frac{c_{\theta_I}^2 m_{\mathcal{A}_1}^2}{m_{\mathcal{A}_1}^2 - m_{\nu_{\alpha R}}^2} \ln\frac{m_{\mathcal{A}_1}^2}{m_{\nu_{\alpha R}}^2} + \frac{s_{\theta_R}^2 m_{\mathcal{S}_2}^2}{m_{\mathcal{S}_2}^2 - m_{\nu_{\alpha R}}^2} \ln\frac{m_{\mathcal{S}_2}^2}{m_{\nu_{\alpha R}}^2} \\ &\left. - \frac{s_{\theta_I}^2 m_{\mathcal{A}_2}^2}{m_{\mathcal{A}_2}^2 - m_{\nu_{\alpha R}}^2} \ln\frac{m_{\mathcal{A}_2}^2}{m_{\nu_{\alpha R}}^2} \right). \end{aligned} \qquad (65)$$

With the assumption $\Lambda_2 \gg \Lambda_1 \gg v$, both the $\mathcal{S}_1, \mathcal{A}_1$ mass splitting $(m_{\mathcal{S}_1}^2 - m_{\mathcal{A}_1}^2)/m_{\mathcal{S}_1,\mathcal{A}_1}^2$ and the mixing angles $\theta_{R,I}^2$ are proportional to $\lambda^2 v^2\Lambda_1^2/\Lambda_2^4$. Hence, the observed neutrinos obtain small Majorana masses, $m_\nu \sim (h^\nu)^2\lambda^2 v^2\Lambda_1^3/32\pi^2\Lambda_2^2$, as expected. For example, if $h^\nu \sim 0.01$, $\lambda \sim 0.1$, the observed value $m_\nu \sim 0.1$ eV requires $\Lambda_1 \sim 1$ TeV and $\Lambda_2 \sim 6.5$ TeV.

In the subsequent sections, we will give a combined analysis of phenomenology of both the models in the question.

5 FCNC and collider bounds

5.1 FCNCs

In both models under consideration, the quark families transform differently under $U(1)_X$. This causes the FCNCs at the tree level, which are mediated only by the new neutral gauge boson Z'. Indeed, from the fermion kinetic terms, $\sum_F \bar{F} i \gamma^\mu D_\mu F$, where F runs over fermion multiplets, we extract the couplings of Z' to quarks induced by X-charge,

$$\mathcal{L} \supset -g_X X_{q_a} \bar{q}_a \gamma^\mu q_a Z'_\mu$$
$$= zg_X(\bar{q}_1 \gamma^\mu q_1 + \bar{q}_2 \gamma^\mu q_2 - \bar{q}_3 \gamma^\mu q_3) Z'_\mu, \qquad (66)$$

where q_a labels quarks of either up-types (u_a) or down-types (d_a), and note that all the quarks are vector-like under X. Let us change to the mass basis by the transformation, $q_{aL,R} = [V_{qL,R}]_{ai} q_{iL,R}$, where q_i denotes mass eigenstates of either up-types, $u_i = (u, c, t)$, or down-types, $d_i = (d, s, b)$, and $V_{qL,R}$ are the unitary matrices satisfying $V_{uL}^\dagger M_u V_{uR} = \text{diag}(m_u, m_c, m_t)$ and $V_{dL}^\dagger M_d V_{dR} = \text{diag}(m_d, m_s, m_b)$. We rewrite (66) as

$$\mathcal{L} \supset zg_X \bar{q}_i \gamma^\mu q_i Z'_\mu - 2zg_X [V_{qL}^*]_{3i} [V_{qL}]_{3j} \bar{q}_{iL} \gamma^\mu q_{jL} Z'_\mu$$
$$+ (L \to R), \qquad (67)$$

where i, j are summed. It is easy to see that the last two terms give rise to FCNCs for $i \neq j$. Integrating Z' out, we get related effective interactions,

$$\mathcal{H}_{\text{FCNC}}^{\text{eff}} = \frac{L_{ij}^2}{m_{Z'}^2} (\bar{q}_{iL} \gamma^\mu q_{jL})^2 + 2(LR) + (RR), \qquad (68)$$

where $L_{ij} = -2zg_X [V_{qL}^*]_{3i} [V_{qL}]_{3j}$, and the last two terms differ from the first one only in chiral structures. Further, the above effective couplings are approximated as

$$\frac{L_{ij}^2}{m_{Z'}^2} \simeq \frac{1}{\bar{\Lambda}^2} ([V_{qL}^*]_{3i} [V_{qL}]_{3j})^2, \qquad (69)$$

where we have defined $\bar{\Lambda}^2 \equiv \Lambda^2$ for the conventional $U(1)_X$ model, while $\bar{\Lambda}^2 \equiv 16\Lambda_1^2 + 25\Lambda_2^2$ for the alternative $U(1)_X$ model.

The effective interactions in (68) contribute to the relevant neutral-meson mixing amplitudes. Assuming the new physics effects dominantly comes from the first term in (68), the existing data imply corresponding bounds,

$$\frac{L_{12}^2}{m_{Z'}^2} < \left(\frac{1}{10^4 \text{ TeV}}\right)^2, \qquad \frac{L_{13}^2}{m_{Z'}^2} < \left(\frac{1}{500 \text{ TeV}}\right)^2,$$
$$\frac{L_{23}^2}{m_{Z'}^2} < \left(\frac{1}{100 \text{ TeV}}\right)^2, \qquad (70)$$

according to K^0-$\bar{K}^0$ mixing, B_d^0-$\bar{B}_d^0$ mixing, and B_s^0-$\bar{B}_s^0$ mixing, respectively [33,34]. Additionally, aligning quark mixing to the down sector, i.e. $V_{uL} = 1$, the CKM matrix is given by $V_{\text{CKM}} = V_{uL}^\dagger V_{dL} = V_{dL}$, thus $[V_{dL}]_{31} = 0.00857$, $[V_{dL}]_{32} = 0.04110$, and $[V_{dL}]_{33} = 0.999118$ [4], which lead to the constraints,

$$\bar{\Lambda} \gtrsim 3.52 \text{ TeV}, \qquad \bar{\Lambda} \gtrsim 4.28 \text{ TeV}, \qquad \bar{\Lambda} \gtrsim 4.11 \text{ TeV}, \quad (71)$$

corresponding to the mentioned meson mixing systems.

Generically, the last two terms of (68) also contribute to the neutral-meson mixing amplitudes through switching on the right-handed quark mixing matrix, V_{qR}. Since V_{qR} is left arbitrarily as in the standard model, we assume $V_{qR} \simeq V_{qL}$ for simplicity and also the reason that the current gauge symmetry that contains B, L may obey a left-right symmetry at high energy. The contribution arising from all effective interactions in (68) to the mass splitting in K^0-$\bar{K}^0$ mixing system, where $(q_i, q_j) = (d, s)$, is given by

$$\Delta m_K|_{\text{NP}} = 2\text{Re}\langle K^0 | \mathcal{H}_{\text{FCNC}}^{\text{eff}} | \bar{K}^0 \rangle$$
$$= 2\text{Re}\langle K^0 | \frac{L_{12}^2}{m_{Z'}^2} (\bar{d}_L \gamma^\mu s_L)^2 + 2\frac{L_{12}R_{12}}{m_{Z'}^2} (\bar{d}_L \gamma^\mu s_L)$$
$$\times (\bar{d}_R \gamma_\mu s_R) + \frac{R_{12}^2}{m_{Z'}^2} (\bar{d}_R \gamma^\mu s_R)^2 | \bar{K}^0 \rangle. \qquad (72)$$

The related hadronic matrix elements are

$$\langle K^0 | (\bar{d}_L \gamma^\mu s_L)^2 | \bar{K}^0 \rangle = \langle K^0 | (\bar{d}_R \gamma^\mu s_R)^2 | \bar{K}^0 \rangle = \frac{1}{3} m_K f_K^2, \qquad (73)$$

$$\langle K^0 | (\bar{d}_L \gamma^\mu s_L)(\bar{d}_R \gamma_\mu s_R) | \bar{K}^0 \rangle$$
$$= -\frac{1}{2} \left[\frac{1}{2} + \frac{1}{3} \left(\frac{m_K}{m_d + m_s} \right)^2 \right] m_K f_K^2, \qquad (74)$$

which have been determined in the vacuum insertion approximation using PCAC [35], in agreement with [28]. Hence,

$$\Delta m_K|_{\text{NP}} \simeq \frac{2m_K f_K^2}{3m_{Z'}^2}$$
$$\text{Re} \left\{ L_{12}^2 - \left[\frac{3}{2} + \left(\frac{m_K}{m_d + m_s} \right)^2 \right] L_{12}R_{12} + R_{12}^2 \right\}. \qquad (75)$$

Similarly for $B_{d,s}^0$-$\bar{B}_{d,s}^0$ mixings with $(q_i, q_j) = (d, b)$ and (s, b), respectively, we have

$$\Delta m_{B_d}|_{\text{NP}} \simeq \frac{2m_{B_d} f_{B_d}^2}{3m_{Z'}^2}$$
$$\text{Re} \left\{ L_{13}^2 - \left[\frac{3}{2} + \left(\frac{m_{B_d}}{m_d + m_b} \right)^2 \right] L_{13}R_{13} + R_{13}^2 \right\}, \qquad (76)$$

$$\Delta m_{B_s}|_{\text{NP}} \simeq \frac{2m_{B_s} f_{B_s}^2}{3m_{Z'}^2}$$
$$\text{Re} \left\{ L_{23}^2 - \left[\frac{3}{2} + \left(\frac{m_{B_s}}{m_s + m_b} \right)^2 \right] L_{23}R_{23} + R_{23}^2 \right\}. \qquad (77)$$

Note that the theoretical predictions of meson mass differences can be decomposed as

$$\Delta m_{K,B_d,B_s} = \Delta m_{K,B_d,B_s}|_{SM} + \Delta m_{K,B_d,B_s}|_{NP}, \quad (78)$$

where the first part/term comes from the SM contribution [36,37],

$$\Delta m_K|_{SM} = 3.074 \times 10^{-12} \text{ MeV}, \quad (79)$$

$$\Delta m_{B_d}|_{SM} = (3.574 \pm 0.191) \times 10^{-10} \text{ MeV}, \quad (80)$$

$$\Delta m_{B_s}|_{SM} = (1.2355 \pm 0.0566) \times 10^{-8} \text{ MeV}, \quad (81)$$

while the second part/term is due to the new physics contribution as derived in (75), (76), and (77). These theoretical predictions will be compared with the experimental values as summarized in [4], namely

$$\Delta m_K|_{exp} = (3.484 \pm 0.006) \times 10^{-12} \text{ MeV}, \quad (82)$$

$$\Delta m_{B_d}|_{exp} = (3.334 \pm 0.013) \times 10^{-10} \text{ MeV}, \quad (83)$$

$$\Delta m_{B_s}|_{exp} = (1.1693 \pm 0.0004) \times 10^{-8} \text{ MeV}. \quad (84)$$

However, due to the presence of long-distance effects in Δm_K, the uncertainties in this system are very large. We therefore require the theory to produce the data for kaon mass difference within $\pm 30\%$, i.e., $0.7 < \Delta m_K|_{SM}/\Delta m_K|_{exp} < 1.3$, or equivalently

$$-0.3 < \frac{\Delta m_K|_{NP}}{\Delta m_K|_{exp}} < 0.3, \quad (85)$$

in agreement with [38]. For the $B_{d,s}$-meson mass differences, the SM predictions are more accurate than that of kaon, so we can calculate the 2σ ranges by combining quadrature of the relative errors in the SM predictions and measurements as

$$0.83 < \frac{\Delta m_{B_d}|_{exp}}{\Delta m_{B_d}|_{SM}} < 1.04, \quad 0.86 < \frac{\Delta m_{B_s}|_{exp}}{\Delta m_{B_s}|_{SM}} < 1.03, \quad (86)$$

and then we obtain the following constraints,

$$-0.17 < \frac{\Delta m_{B_d}|_{NP}}{\Delta m_{B_d}|_{SM}} < 0.04,$$

$$-0.14 < \frac{\Delta m_{B_s}|_{NP}}{\Delta m_{B_s}|_{SM}} < 0.03. \quad (87)$$

By using the following input parameters [4,39,40], in units of MeV,

$$m_d = 4.67, \quad m_s = 93.4, \quad m_b = 4180, \quad (88)$$

$$m_K = 497.611, \quad m_{B_d} = 5279.66, \quad m_{B_s} = 5366.92, \quad (89)$$

$$f_K = 155.7, \quad f_{B_d} = 190.5, \quad f_{B_s} = 230.7, \quad (90)$$

we obtain the constraints

$$\bar\Lambda \gtrsim 4.91 \text{ TeV}, \quad \bar\Lambda \gtrsim 12.97 \text{ TeV}, \quad \bar\Lambda \gtrsim 14.14 \text{ TeV}, \quad (91)$$

corresponding to the K^0-$\bar K^0$, B_d^0-$\bar B_d^0$, and B_s^0-$\bar B_s^0$ mixing systems. These lower bounds are generally more stringent and are quite larger than the those determined in (71).[2]

Alternatively, one could align the quark mixing to the up quark sector by assuming $V_{dL} = 1$ and then $V_{CKM} = V_{uL}^\dagger V_{dL} = V_{uL}^\dagger$. Hence, the current D^0-$\bar D^0$ mixing data implies

$$\frac{[V_{CKM}]_{13}[V_{CKM}^*]_{23}}{\bar\Lambda} < \frac{1}{10^3 \text{ TeV}}, \quad (92)$$

given that the first term in Eq. (68) dominantly contributes to the relative meson mixing amplitude [33,34]. Taking $[V_{CKM}]_{13} = 0.00369$ and $[V_{CKM}^*]_{23} = 0.04182$ [4], we obtain a constraint $\bar\Lambda \gtrsim 0.15$ TeV, which is much weaker than those obtained in Eq. (71). Further, the mass splitting in this system has the form similar to Eq. (75), i.e.

$$\Delta m_D|_{NP} \simeq \frac{2m_D f_D^2}{3m_{Z'}^2}$$

$$\text{Re}\left\{ L_{12}^2 - \left[\frac{3}{2} + \left(\frac{m_D}{m_u + m_c} \right)^2 \right] L_{12} R_{12} + R_{12}^2 \right\}, \quad (93)$$

if all the terms in Eq. (68) for contribution [42]. For this scenario, using the input values given in MeV as [4,40],

$$\Delta m_D|_{exp} = (6.56237 \pm 0.76353) \times 10^{-12}, \quad (94)$$

$$m_D = 1864.84, \quad f_D = 211.6, \quad m_u = 2.16,$$

$$m_c = 1270, \quad (95)$$

and requiring $-0.3 < \Delta m_D|_{NP}/\Delta m_D|_{exp} < 0.3$ as done in the K^0-$\bar K^0$ mixing system, we get a corresponding constraint as $\bar\Lambda \gtrsim 1.04$ TeV, which is also much weaker than those obtained in Eq. (91).

5.2 LEP-II

The LEP experiments have made measurements in electron-positron collisions with collision center-of-mass energy ranging from the Z pole (LEP-I) up to 209 GeV (LEP-II), providing stringent constraints on Z' boson [43,44]. One of the processes searched at the LEP experiments is the four-fermion contact interaction mediated by heavy Z'

---

[2] At low energy, Z' may also contribute to atomic parity violation but would be safely suppressed by the current FCNC bound (see, [41], for a discussion).

boson, which can be parameterized by the following effective Lagrangian [45],

$$\mathcal{L}_{\text{eff}} = \frac{1}{1+\delta_{ef}} \frac{1}{m_{Z'}^2} \sum_{i,j=L,R} C_{e_i}^{Z'} C_{f_j}^{Z'} \bar{e}_i \gamma_\mu e_i \bar{f}_j \gamma^\mu f_j, \quad (96)$$

where $\delta_{ef} = 1(0)$ for $f = e$ ($f \neq e$). From the relevant data of the LEP-II experiment [44], we impose a constraint on this contact interaction as

$$\frac{2\sqrt{2\pi} m_{Z'}}{\sqrt{(C_{e_L}^{Z'})^2 + (C_{e_R}^{Z'})^2}} \gtrsim 24.6 \text{ TeV}. \quad (97)$$

Note that the electron is vector-like under $U(1)_X$, i.e. $C_{e_L}^{Z'} = C_{e_R}^{Z'} = C_e^{Z'} = -zg_X$, for both models under consideration. Therefore, we get a lower bound of the new physics scale, $\bar{\Lambda} \gtrsim 3.47$ TeV, which is independent of g_X and z and is quite smaller than the bounds obtained from FCNCs, shown in Eq. (91).

5.3 LHC

At the LHC experiment, the new gauge boson Z' can be resonantly produced via the fusion processes $\bar{q}q \to Z'$ in which q indicates the SM quarks, and this boson subsequently decays into the SM fermions as well as the exotic particles if kinetically allowed. Furthermore, the most significant decay channel of Z' is given by $Z' \to l^+l^-$ with $l = e, \mu, \tau$ because of well-understood backgrounds [46] and also that it signifies a Z' having both couplings to lepton and quark like ours. Using the narrow width approximation, the cross section for the relevant process takes the form,

$$\sigma(pp \to Z' \to l^+l^-) \simeq \sigma(pp \to Z')\text{Br}(Z' \to l^+l^-). \quad (98)$$

The first factor is the production cross section of the Z' boson, which can be estimated as

$$\sigma(pp \to Z') = \sum_q L_{q\bar{q}}(m_{Z'}^2)\hat{\sigma}(\bar{q}q \to Z'), \quad (99)$$

where $L_{q\bar{q}}$ is the parton luminosity,

$$L_{q\bar{q}}(m_{Z'}^2) = \int_{\frac{m_{Z'}^2}{s}}^1 \frac{dx}{xs} \left[f_q(x, m_{Z'}^2) f_{\bar{q}} \left(\frac{m_{Z'}^2}{xs}, m_{Z'}^2 \right) \right. $$
$$\left. + f_q \left(\frac{m_{Z'}^2}{xs}, m_{Z'}^2 \right) f_{\bar{q}}(x, m_{Z'}^2) \right], \quad (100)$$

with $\sqrt{s}$ to be the collider center-of-mass energy and $f_{q(\bar{q})}(x, m_{Z'}^2)$ to be the parton distribution function of the quark q (antiquark $\bar{q}$) evaluated at the scale $m_{Z'}^2$, while the partonic cross section is approximated as $\hat{\sigma}(\bar{q}q \to Z') \simeq \frac{\pi}{3}(C_q^{Z'})^2$. The last factor in Eq. (98) is the branching ratio of Z' decaying into the lepton pair l^+l^-,

$$\text{Br}(Z' \to l^+l^-) = \frac{\Gamma(Z' \to l^+l^-)}{\Gamma_{Z'}}, \quad (101)$$

where the partial decay width of Z' boson is approximately given by

$$\Gamma(Z' \to l^+l^-) \simeq \frac{m_{Z'}}{12\pi}(C_l^{Z'})^2, \quad (102)$$

while the total Z' decay width is estimated as

$$\Gamma_{Z'} \simeq \frac{m_{Z'}}{12\pi} \sum_f N_C(f)(C_f^{Z'})^2 + \frac{m_{Z'}}{8\pi}(C_{v_L}^{Z'})^2$$
$$+ \frac{m_{Z'}}{24\pi}(C_{v_R}^{Z'})^2 \sum_{i=1}^3 \left(1 - \frac{4m_{v_{iR}}^2}{m_{Z'}^2}\right)^{3/2} \Theta\left(\frac{m_{Z'}}{2} - m_{v_{iR}}\right)$$
$$+ \frac{m_{Z'}}{12\pi}(C_\xi^{Z'})^2 \left(1 - \frac{4m_\xi^2}{m_{Z'}^2}\right)^{3/2} \Theta\left(\frac{m_{Z'}}{2} - m_\xi\right)$$
$$+ \frac{m_{Z'}}{48\pi}(zg_X)^2 \left(1 - \frac{4m_\eta^2}{m_{Z'}^2}\right)^{3/2} \Theta\left(\frac{m_{Z'}}{2} - m_\eta\right), \quad (103)$$

for the conventional $U(1)_X$ model, assuming $m_{Z'} < m_{H'}$, and

$$\Gamma_{Z'} \simeq \frac{m_{Z'}}{12\pi} \sum_f N_C(f)(C_f^{Z'})^2 + \frac{m_{Z'}}{8\pi}(C_{v_L}^{Z'})^2$$
$$+ \frac{m_{Z'}}{12\pi}(C_{v_{\alpha R}}^{Z'})^2 + \frac{m_{Z'}}{48\pi}(-8zg_X)^2$$
$$+ \frac{m_{Z'}}{24\pi}(C_{v_{3R}}^{Z'})^2 \left(1 - \frac{4m_{v_{3R}}^2}{m_{Z'}^2}\right)^{3/2} \Theta\left(\frac{m_{Z'}}{2} - m_{v_{3R}}\right), \quad (104)$$

for the alternative $U(1)_X$ model, assuming that Z' is lighter than the new Higgs bosons H_2, $\mathcal{S}_{1,2}$, and $\mathcal{A}_{1,2}$. Above, f denotes the SM charged fermions, N_f is the color number of the fermion f, Θ is the step function, and the related couplings are given by

$$C_{e,\mu,\tau}^{Z'} = -C_{u,c,d,s}^{Z'} = C_{t,b}^{Z'} = C_{v_L}^{Z'} = C_{v_R}^{Z'} = \frac{1}{2}C_\xi^{Z'}$$
$$= \frac{1}{4}C_{v_{\alpha R}}^{Z'} = -\frac{1}{5}C_{v_{3R}}^{Z'} = -zg_X. \quad (105)$$

Employing the MSTW2008 parton distribution functions [47] and setting $\sqrt{s} = 13$ TeV, we plot the cross-section for the relevant process as a function of the Z' boson mass, for various values of the product $|z|g_X$, which are shown in Fig. 2. The left panel corresponds to the convention $U(1)_X$ model, assuming $m_{v_{iR}} = 2m_\xi/3 = 4m_\eta/3 = m_{Z'}/3$, while the right panel corresponds to the alternative $U(1)_X$ model, given that $m_{v_{3R}} = m_{Z'}/2$. In addition, in each of these panels, we include the upper limits on the cross section of this process observed by ATLAS [46] and CMS [48] experiments. In the left (right) panel, the lower bounds on the Z' boson mass are 4.5, 4.9, and 5.3 (4.0, 4.5, and 4.9) TeV according to $|z|g_X = 0.1, 0.15,$ and 0.22.

In Fig. 3, the lower bounds of Z' boson mass that obtain from the ATLAS (CMS) are described by the black (gray)
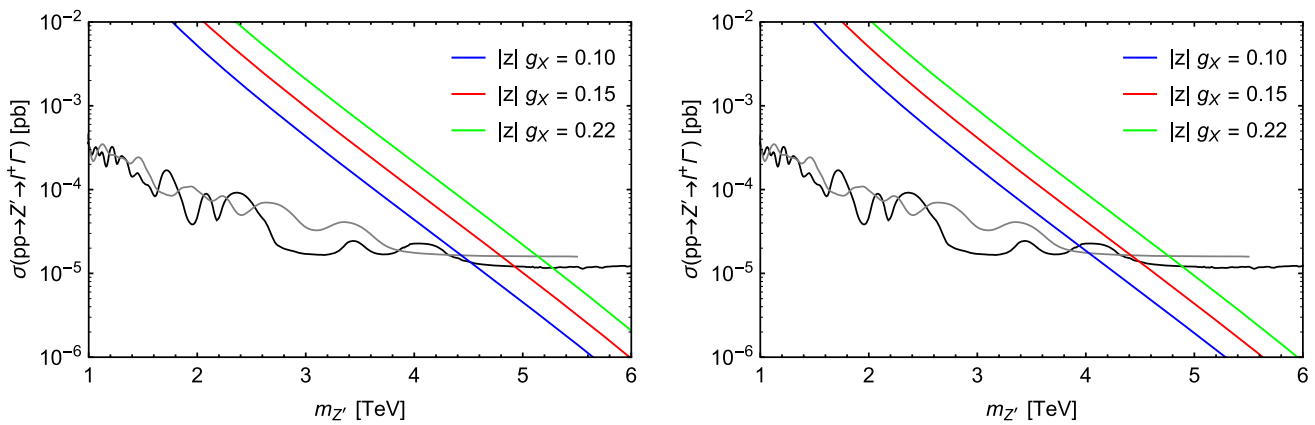
Fig. 2 Dilepton production cross-section as a function of the Z' boson mass for various values of the $|z|g_X$ product. The left (right) panel corresponds to the conventional (alternative) $U(1)_X$ model. The black curve. The left (right) panel corresponds to the convention (alternative) $U(1)_X$ model. For comparison, in each of these panels, we also add the lower bounds on the Z' boson mass which come from the FCNCs (brown line) and the LEP-II (purple line). The available regions for the Z' boson mass lie above these four lines. It is easy to see that the constraint from the ATLAS and CMS (FCNCs) is the strongest if the coupling strength $|z|g_X$ is smaller (larger) than about 0.18 for the convention $U(1)_X$ model and 0.16 for the alternative $U(1)_X$ model.

(gray) curve shows the upper bound on the cross-section obtained by the ATLAS 2019 results for $\Gamma/m = 3\%$ [46] (the CMS 2019 results [48] for $\Gamma/m = 0.6\%$)

6 Dark matter phenomenology

6.1 Single-component dark matter in the conventional $U(1)_X$ model

As shown, the dark matter candidate in the model, i.e., the lightest field of ξ and η, can possess an arbitrary mass, which is stabilized due to the conservation of the Z_2 residual symmetry, $p = (-1)^{X/z+2s}$. Additionally, the observed light neutrino masses require the new physics scale Λ either in the TeV region or close to the grand unification scale, depending on magnitude of the Yukawa couplings, h^ν and f^ν. Hence, the model predicts two different scenarios of dark matter production.

1. If the new physics scale is at the TeV region, the freeze-out mechanism works and defines not only the dark matter relic density through its annihilation into the SM particles as well as others when kinematically allowed, but also the dark matter nature to be a weakly interacting massive particle (WIMP).
2. If the new physics scale is of order the grand unification or around, the dark matter may be asymmetrically pro-

duced from the CP-violation decay of the right-handed neutrinos, via complex couplings $y_a \bar{\xi}_L \eta \nu_{aR}$, similar to the leptogenesis mechanism for lepton asymmetry generation.

However, only the first scenario is considered in this work due to the potential discovery of new physics at the LHC.

6.1.1 Dark matter as a fermion ξ

Assume that the fermion ξ is lighter than the scalar η. Then ξ is stabilized, responsible for dark matter. Because ξ is charged under $U(1)_X$, its pair annihilation into the SM particles and others (if kinematically allowed) in the early universe proceeds dominantly through s-channel exchange diagrams mediated by the new gauge boson Z'. Hence, the dark matter annihilation cross section times relative velocity is estimated as

$$
\langle \sigma v_{\text{rel}} \rangle_{\xi\xi^c \to \text{all}} \simeq \frac{(C_\xi^{Z'})^2 m_\xi^2}{\pi (4m_\xi^2 - m_{Z'}^2)^2}
$$
$$
\times \left[\sum_f N_C(f)(C_f^{Z'})^2 + \frac{3(C_{\nu_L}^{Z'})^2}{2} \right.
$$
$$
+ \frac{(C_{\nu_R}^{Z'})^2}{2} \sum_{i=1}^{3} \left(1 - \frac{m_{\nu_{iR}}^2}{4m_\xi^2} \right)
$$
$$
\left. \times \left(1 - \frac{m_{\nu_{iR}}^2}{m_\xi^2} \right)^{1/2} \Theta(m_\xi - m_{\nu_{iR}}) \right],
$$

(106)

where f denotes the SM charged fermions, N_f is the color number of the fermion f, Θ is the step function, and the related couplings are shown in Eq. (105). Hence, the relic
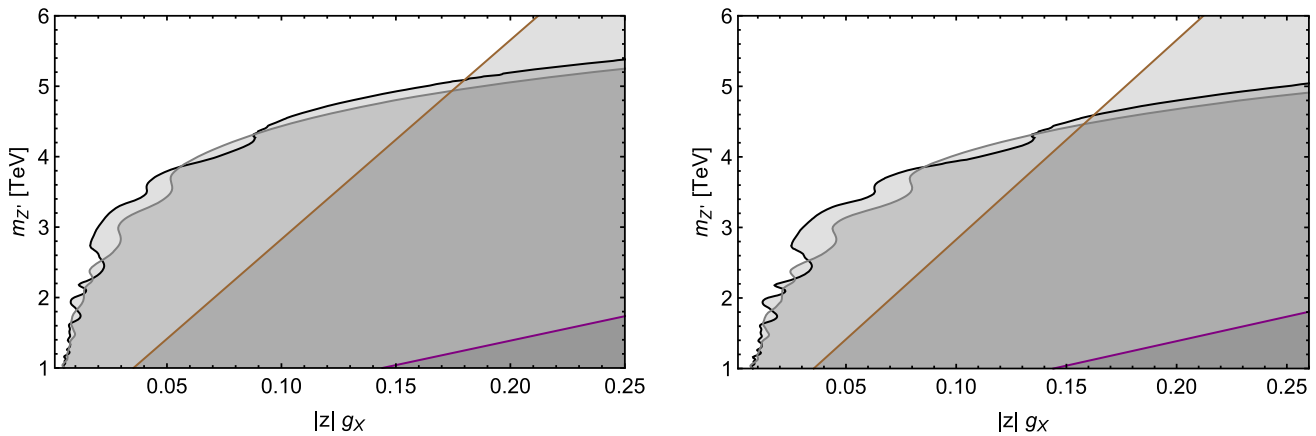
Fig. 3 The left (right) panel corresponds to the conventional (alternative) $U(1)_X$ model. For each panel, the black (gray), brown, and purple lines denote the lower bounds on the Z' boson mass obtained from the Z' boson search by the ATLAS (CMS) collaboration, the FCNCs, and the LEP-II dilepton signal constraint, respectively. The parameter space according to shaded regions is excluded

abundance of fermion dark matter is given by

$$\Omega_\xi h^2 \simeq \frac{0.1 \text{ pb}}{\langle \sigma v_{\text{rel}} \rangle_{\xi \xi^c \to \text{all}}}. \tag{107}$$

Let $\Lambda = 15$ (45) TeV satisfy the limits from the FCNCs and the LEP-II (a future projected bound), and take $m_{v_{iR}} = m_{Z'}/3$. According to $\Lambda = 15$ (45) TeV, we make the blue (red) contours of the correct dark matter relic density, i.e. $\Omega_\xi h^2 \simeq 0.12$ [1], as shown in the left panel in Fig. 4. Added to these density contours are the black (dashed black) and gray (dashed gray) lines corresponding to $|z|g_X \simeq 0.168$ (0.038) and $|z|g_X \simeq 0.162$ (0.035) which are extracted from the ATLAS and CMS limits at $\Lambda = 15$ (45) TeV, respectively, where notice that the shaded regions are excluded. From here, we obtain the lower bound for fermion dark matter mass to be $m_\xi \gtrsim 2.1$ (1.7) TeV for $\Lambda = 15$ (45) TeV.

Besides the correct dark matter relic density, the fermion candidate is constrained by the direct dark matter detection experiments which measure the scattering cross section of the dark matter on nucleons in target nucleus. At the microscopic level, the scattering of the dark matter on nucleons can be described by effective interactions between the dark matter and the SM quarks. In the model under consideration, such interactions are dominantly contributed by t-channel diagrams by the new gauge boson Z' exchange, given by

$$\mathcal{L}_{\xi-\text{quark}}^{\text{eff}} = \frac{1}{m_{Z'}^2} C_\xi^{Z'} C_q^{Z'} (\bar{\xi} \gamma^\mu \xi)(\bar{q} \gamma_\mu q), \tag{108}$$

where $q = u, d$. Note that both ξ and the SM quarks are vector-like under $U(1)_X$. Hence, we obtain the spin-independent (SI) scattering cross section of ξ on a nucleon,

labeled as $\mathcal{N}$ with corresponding mass $m_\mathcal{N}$, such as [49]

$$\sigma_\xi^{\text{SI}} = \frac{9 \mu_{\xi \mathcal{N}}^2}{4\pi} \frac{1}{m_{Z'}^4} (C_\xi^{Z'})^2 (C_u^{Z'})^2$$

$$\simeq 1.377 \times 10^{-45} \left(\frac{m_\mathcal{N}}{1 \text{ GeV}} \right)^2 \left(\frac{15 \text{ TeV}}{\Lambda} \right)^4 \text{ cm}^2, \tag{109}$$

which is independent of the product $|z|g_X$. Above, $\mu_{\xi \mathcal{N}} = m_\xi m_\mathcal{N}/(m_\xi + m_\mathcal{N}) \simeq m_\mathcal{N}$ is the reduced mass of the dark matter-nucleon system.

Taking $m_\mathcal{N} \simeq 1$ GeV and $\Lambda = 15$ TeV as before, the model predicts $\sigma_\xi^{\text{SI}} \simeq 1.377 \times 10^{-45}$ cm^2 as described by the blue line in the right panel in Fig. 4, which agrees with the current bound from XENON1T [50] (LZ [51]) that is described by the gray (black) curve, if dark fermion mass satisfies $m_\xi \gtrsim 3.0$ (4.9) TeV. These lower bounds for the fermion dark matter mass are generally stricter than that obtained from the correct density constraint. Further, we include the projected bounds from upcoming direct detection experiments such as XENONnT [52], LZ [53], and DARWIN [54], which are respectively described by the gray, black, and brown dotted curves. It is clear that these bounds constrain the new physics scale and/or the dark fermion mass to higher values. Take an example, the model predicts $\sigma_\xi^{\text{SI}} \simeq 1.7 \times 10^{-47}$ cm^2 for $\Lambda = 45$ TeV as descried by the red line, which agrees with the projected bounds if dark fermion mass satisfies $m_\xi \gtrsim 7.9$ TeV.

6.1.2 Dark matter as a scalar η

Alternatively, we consider a possibility that the dark scalar singlet η is lighter than the dark fermion ξ. So, η is stabilized, responsible for dark matter. For simplicity, we assume that η is lighter than H', Z', and v_{iR}, and thus it annihilates only to SM particles in the early universe. Such annihila-
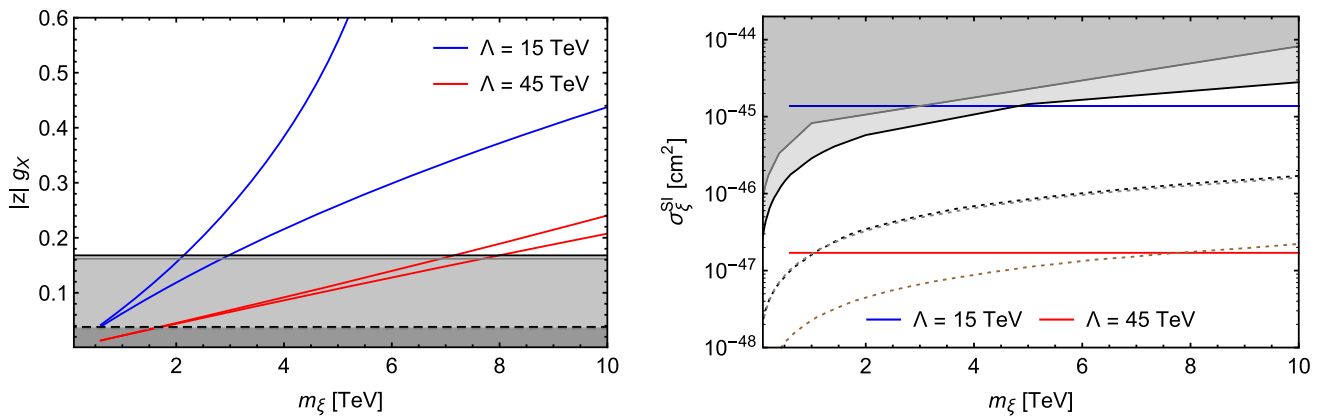
Fig. 4 In the left panel, we make the blue (red) contours of the correct dark matter relic density at $\Lambda = 15\,(45)$ TeV. In the right panel, we make the blue (red) lines of the SI scattering cross section of the dark fermion on a nucleon at $\Lambda = 15\,(45)$ TeV. The shaded regions are excluded by the current experiments. The dotted curves are the projected bounds

tion may proceed through a contact interaction with the SM Higgs fields as well as H, H', and Z' portals. However, the contribution of Z' portal to dark matter observables is quite similar to the case of the fermion dark matter above, whereas the H' portal does not contribute to direct dark matter detection. Hence, we do not consider these two portals here, given that the contributions of these two portals are negligible, by imposing appropriate parameters. With the contact interaction and H portal, the dark matter pair annihilation into the SM particles is given by the following dominant channels:

$$\eta^*\eta \to HH, W^+W^-, ZZ, \tag{110}$$

yielding the dark matter annihilation cross section times relative velocity to be

$$\langle \sigma v_{\rm rel} \rangle_{\eta^*\eta \to \rm SM\,SM} \simeq \frac{\lambda_5^2}{16\pi m_\eta^2}. \tag{111}$$

Assuming that the scalar dark matter η provides a correct relic density, i.e. $\Omega_\eta h^2 \simeq 0.1\,{\rm pb}/\langle \sigma v_{\rm rel} \rangle_{\eta^*\eta \to \rm SM\,SM} \simeq 0.12$, we derive the dark matter mass at the TeV regime, i.e.

$$m_\eta \simeq |\lambda_5| \times 3.05\,\text{TeV}. \tag{112}$$

Concerning the direct dark matter detection, the effective Lagrangian that describes the interaction between η and the SM quarks induced by t-channel exchange diagrams of the new Higgs boson H is given by

$$\mathcal{L}_{\eta-\rm quark}^{\rm eff} = \frac{\lambda_5 m_q}{m_H^2}\eta^*\eta\bar{q}q \tag{113}$$

with q denotes ordinary quarks. From this Lagrangian, we acquire the SI scattering cross section of η on a nucleon, such as [55]

$$\sigma_\eta^{\rm SI} = \left(\frac{\lambda_5}{2\sqrt{\pi}} \frac{\mu_{\eta\mathcal{N}}}{m_H^2} \frac{m_\mathcal{N}}{m_\eta} C_\mathcal{N} \right)^2, \tag{114}$$

where $\mu_{\eta\mathcal{N}} = m_\eta m_\mathcal{N}/(m_\eta + m_\mathcal{N}) \simeq m_\mathcal{N}$, and

$$C_\mathcal{N} = \frac{2}{9} + \frac{1}{A}\sum_{q=u,d,s}\left[\left(Z - \frac{2}{9}A\right)f_q^p + (A - Z)f_q^n\right], \tag{115}$$

in which Z is the nucleus charge, A is the total number of nucleons in the nucleus, and $f_q^{p(n)}$ are the scalar couplings of the nucleon to $q = u, d, s$. The values of $f_q^{p(n)}$ are given by [56,57]

$$f_u^{p(n)} \simeq 0.0208(0.0189), \qquad f_d^{p(n)} \simeq 0.0411(0.0451),$$
$$f_s^{p(n)} \simeq 0.043(0.043). \tag{116}$$

Taking $A = 131$, $Z = 54$, $m_\mathcal{N} \simeq 1$ GeV, and $m_H \simeq 125.25$ GeV [4], we estimate

$$\sigma_\eta^{\rm SI} \simeq 1.259 \times 10^{-45}\left(\frac{|\lambda_5| \times 3.05\,\text{TeV}}{m_\eta}\right)^2\,\text{cm}^2. \tag{117}$$

This result implies that the scalar dark matter η with a mass at TeV regime, $m_\eta \simeq |\lambda_5| \times 3.05$ TeV, yields both the correct relic density and the current exclusion limit in direct dark matter detection experiments [50,58,59].

6.2 Two-component dark matter in the alternative $U(1)_X$ model

As shown in the Sect. 4.2, the alternative $U(1)_X$ model provides two candidates for dark matter simultaneously, the one being ν_{3R} accidentally stabilized and the remainder to be the lightest of Z_2-odd fields ($\nu_{\alpha R}$, ϕ, η) stabilized by $p = (-1)^{X/z+2s}$. With the assumption $\Lambda_2 \gg \Lambda_1$ as discussed in the previous subsections, the Z_2-odd physical scalars are generally much heavier than $\nu_{\alpha R}$. Hence, the light-
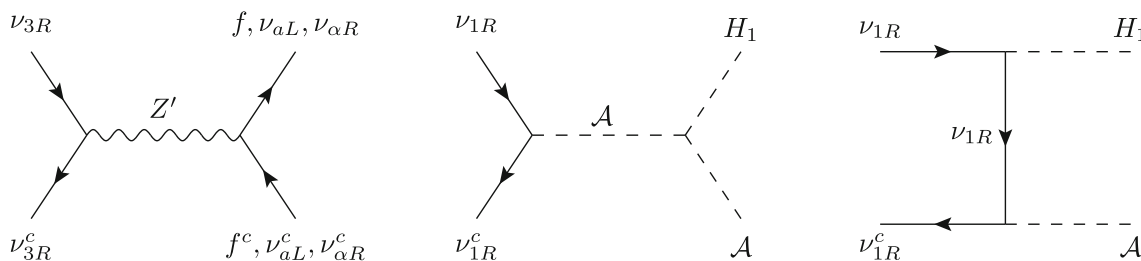
Fig. 5 Dominant contributions to annihilation of the two-component fermion dark matter

est particle of $\nu_{\alpha R}$, such as ν_{1R} without loss of generality, and ν_{3R} play the role of two-component dark matter candidates.

The dominant channels in the dark matter pair annihilation of ν_{3R} (ν_{1R}), if allowed by kinematics, are $\nu_{3R}\nu_{3R}^c \to ff^c, \nu_{aL}\nu_{aL}^c, \nu_{\alpha R}\nu_{\alpha R}^c, H_\alpha H_\alpha, \mathcal{A}\mathcal{A}, \mathcal{S}_\alpha \mathcal{S}_\alpha, \mathcal{A}_\alpha \mathcal{A}_\alpha, Z'H_\alpha, Z'\mathcal{S}_\alpha, Z'\mathcal{A}_\alpha, Z'Z'$ ($\nu_{1R}\nu_{1R}^c \to ff^c, \nu_{aL}\nu_{aL}^c, H_1 H_1, \mathcal{A}\mathcal{A}, H\mathcal{A}, H_1\mathcal{A}$) with f indicates the SM charged fermions, which are proceeded via the s-channel interchange of new gauge boson Z' and new scalar H_2 ($H_1, \mathcal{A}$), and via the t-channel of ν_{3R} ($\nu_{1R}, \phi_1^0, \phi_2^-$). However, this work assuming $\Lambda_2 \gg \Lambda_1 \gg v$, so only some annihilation channels of them are allowed. Additionally, for for the sake of simplicity, we assume that the relic density of ν_{3R} is governed mainly by s-channel exchange diagrams of Z', while the pair annihilation processes of ν_{1R} are proceed dominantly though s- and t-channel exchange diagrams of $\mathcal{A}$ and ν_{1R} respectively, which are shown in Fig. 5. Here, there is the conversion between dark matter components, namely the heavier dark matter component ν_{3R} annihilates into the lighter one ν_{1R}.

In the non-relativistic approximation, the thermal average annihilation cross-section times relative velocity for each dark matter component is estimated as

$$\langle \sigma v \rangle_{\nu_{1R}^c \nu_{1R} \to H_1 \mathcal{A}} \simeq \frac{(f_{11}^\nu)^2 |4m_{\nu_{1R}}^2 - m_{H_1}^2|}{512\pi m_{\nu_{1R}}^4}$$
$$\times \left(|f_{11}^\nu| + \frac{\lambda_1 \Lambda_1}{2m_{\nu_{1R}}} \right)^2, \quad (118)$$

$$\langle \sigma v \rangle_{\nu_{3R}^c \nu_{3R} \to \text{all}} \simeq \frac{(C_{\nu_{3R}}^{Z'})^2 m_{\nu_{3R}}^2}{4\pi (4m_{\nu_{3R}}^2 - m_{Z'}^2)^2}$$
$$\times \left[\sum_f N_C(f)(C_f^{Z'})^2 \right.$$
$$\left. + \frac{3(C_{\nu_L}^{Z'})^2}{2} + (C_{\nu_{\alpha R}}^{Z'})^2 \right], \quad (119)$$

where f presents the SM charged fermions and the relevant couplings are shown in Eq. (105).

In the two-component dark matter framework, the dark matter relic abundance due to the thermal freeze-out is computed by solving the coupled Boltzmann equations. Assum-

ing that the production of the ν_{1R} component from the ν_{3R} component is less significant compared to its annihilation into the $H_1, \mathcal{A}$ final states, one can obtain the individual relic abundance of each dark matter component through an approximate analytic solution as [60]

$$\Omega_{\nu_{1R}} h^2 = \frac{1.07 \times 10^9 x_{\nu_{1R}}}{\sqrt{g_*} m_P \langle \sigma v \rangle_{\nu_{1R}^c \nu_{1R} \to H_1 \mathcal{A}}},$$
$$\Omega_{\nu_{3R}} h^2 = \frac{1.07 \times 10^9 x_{\nu_{3R}}}{\sqrt{g_*} m_P \langle \sigma v \rangle_{\nu_{3R}^c \nu_{3R} \to \text{all}}}, \quad (120)$$

where $g_* = 106.75$ is the effective total number of degrees of freedom, $x_{\nu_{1,3R}} \simeq 25$ are parameters related to the freeze-out temperature. Hence, the dark matter relic abundance is sum of the individual contributions, namely

$$\Omega_{\text{DM}} h^2 = \Omega_{\nu_{1R}} h^2 + \Omega_{\nu_{3R}} h^2. \quad (121)$$

The relic density of dark matter depends on six parameters, which are $m_{\nu_{1R}}, m_{\nu_{3R}}, f_{11}^\nu, f_{33}^\nu, \lambda_1$, and the product $|z|g_X$. Taking $f_{11}^\nu = f_{33}^\nu = -\sqrt{2}$ and $m_{\nu_{3R}} = 6m_{\nu_{1R}}$, in Fig. 6, we make contours of the correct relic density of dark matter, i.e., $\Omega_{\text{DM}} h^2 \simeq 0.12$ [1], as a function of $m_{\nu_{1R}}$ and λ_1 for different choices of $|z|g_X$ (left panel), of $m_{\nu_{1R}}$ and $|z|g_X$ for different choices of λ_1 (right panel). This figure shows the viable mass region of ν_{1R} in the order $\mathcal{O}(1)$ TeV, and $0.16 \lesssim |z|g_X \lesssim 0.3$. Note that when $m_{\nu_{1R}} = m_{H_1}/2$, equivalently $\lambda_1 = 2$ (with $f_{11}^\nu = -\sqrt{2}$), then $\langle \sigma v \rangle_{\nu_{1R}^c \nu_{1R} \to H_1 \mathcal{A}} = 0$, which suppress the correct density and leads to a disconnected region on each curve in the left panel. In the right panel, when $m_{\nu_{3R}} = m_{Z'}/2$, equivalently $|z|g_X \simeq 0.2$ (with $\Lambda_2 \gg \Lambda_1$), then $\langle \sigma v \rangle_{\nu_{3R}^c \nu_{3R} \to \text{all}} \to \infty$, which reduces the relic density of ν_{3R} to zero, thus the correct relic density of dark matter is only set by the ν_{1R} pair annihilation.

In Fig. 7, we show the contribution ratio of dark matter components to the correct density as a function of $m_{\nu_{1R}}$ for different choices of λ_1, while $m_{\nu_{3R}} = 6m_{\nu_{1R}}$ and $f_{11}^\nu = -\sqrt{2}$ kept fixed. The dashed black line corresponds to a contribution ratio of 0.5. It is easy to see that ν_{1R} dominantly contributes to the correct density when its mass takes on large values in the possible mass region.

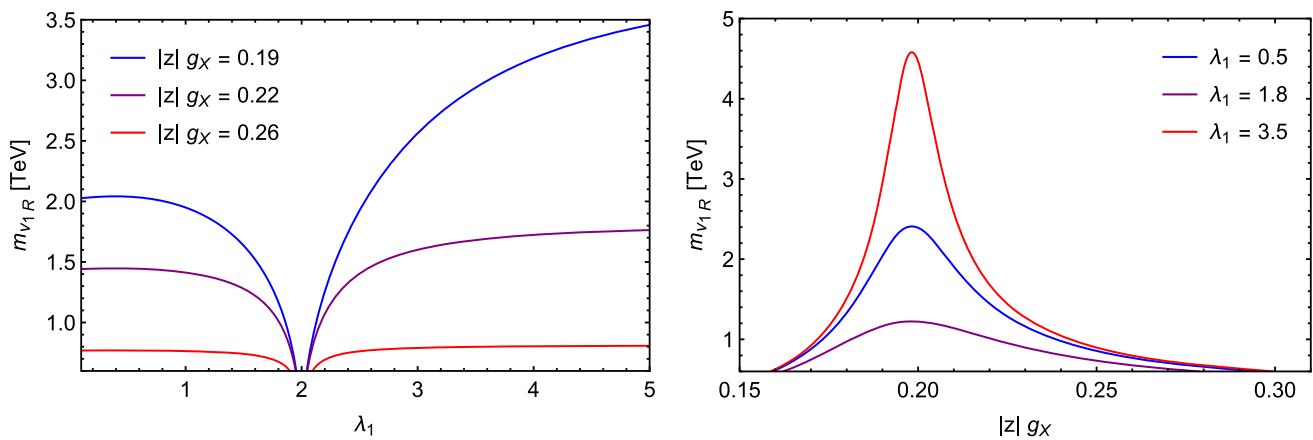Concerning the constraint from the direct detector experiments, it is interesting that two dark matter candidates

Fig. 6 Total dark matter density contoured as functions of dark matter masses and λ_1 (left panel) and $|z|g_X$ (right panel)
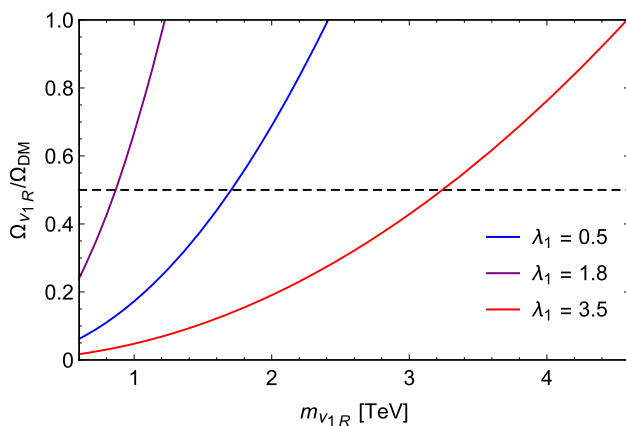

Fig. 7 The contribution ratio of dark matter components to the total density as function of dark matter masses

under consideration are all Majorana fermions, which scatter with nucleon only via spin-dependent (SD) effective interactions by the t-channel exchange of the new gauge boson Z'. Such interactions give the SD scattering cross section of each dark matter candidate on a neutron target, $\sigma_{SD} \sim g_A^{Z'}(\nu_{1,3R})[g_A^{Z'}(u)\lambda_u + g_A^{Z'}(d)(\lambda_d + \lambda_s)]$, where $g_A^{Z'}(f)$ is the axial-vector couplings of Z' to f, while $\lambda_{u,d,s}$ are the fractional quark-spin coefficients [55]. Because the SM quarks are all vector-likes under $U(1)_X$, the axial-vector couplings of Z' to them vanish. Hence, the model predicts a negative search result, as reported by the experiments [61–63].

7 Conclusion

In this work, we have proposed a $U(1)_X$ extension of the SM, where the X charge depends on flavor and is a linear combination of the usual baryon and lepton numbers. By the anomaly cancellation conditions associated with the new charge X, this extension not only explains the existence of only three fermion families as observed but also requires the presence of at least three right-handed neutrinos similar to the SM extension with $U(1)_{B-L}$.

Depending on the X charge assignment for the right-handed neutrinos, we obtain two potential models for this approach, each of them predicts a distinct mechanism for neutrino mass generation, seesaw vs. scotogenic, as well as the dark matter structure, single- vs. two-component(s). Additionally, one of dark matter is stabilized by residual symmetry $p = (-1)^{X/z+2s}$, while the other one of dark matter is accidentally stabilized by the gauge symmetry. Both the models predict the dark matter nature as WIMP(s) with dark matter mass in the TeV regime.

We have also investigated the FCNC and particle collider bounds and predict generically a lower bound for the new physics scale to be roundly 14.14 TeV.

References

1. Planck collaboration, Planck 2018 results. VI. Cosmological parameters, Astron. Astrophys. **641**, A6 (2020). https://doi.org/10.1051/0004-6361/201833910. arXiv:1807.06209
2. T. Kajita, Nobel lecture: discovery of atmospheric neutrino oscillations. Rev. Mod. Phys. **88**, 030501 (2016). https://doi.org/10.1103/RevModPhys.88.030501
3. A.B. McDonald, Nobel lecture: the Sudbury neutrino observatory: observation of flavor change for solar neutrinos. Rev. Mod. Phys. **88**, 030502 (2016). https://doi.org/10.1103/RevModPhys.88.030502
4. Particle Data Group collaboration, Review of particle physics. PTEP **2022**, 083C01 (2022). https://doi.org/10.1093/ptep/ptac097
5. P. Langacker, The physics of heavy Z' gauge bosons. Rev. Mod. Phys. **81**, 1199 (2009). https://doi.org/10.1103/RevModPhys.81.1199. arXiv:0801.1345
6. R. Foot, S. Vagnozzi, Dissipative hidden sector dark matter. Phys. Rev. D **91**, 023512 (2015). https://doi.org/10.1103/PhysRevD.91.023512. arXiv:1409.7174
7. N. Okada, S. Okada, Z'-portal right-handed neutrino dark matter in the minimal U(1)$_X$ extended Standard Model. Phys. Rev. D **95**, 035025 (2017). https://doi.org/10.1103/PhysRevD.95.035025. arXiv:1611.02672
8. N. Okada, S. Okada, D. Raut, Natural Z' -portal Majorana dark matter in alternative U(1) extended standard model. Phys. Rev. D **100**, 035022 (2019). https://doi.org/10.1103/PhysRevD.100.035022. arXiv:1811.11927
9. B. Dutta, S. Ghosh, J. Kumar, A sub-GeV dark matter model. Phys. Rev. D **100**, 075028 (2019). https://doi.org/10.1103/PhysRevD.100.075028. arXiv:1905.02692
10. G. Choi, M. Suzuki, T.T. Yanagida, Degenerate fermion dark matter from a broken $U(1)_{B-L}$ gauge symmetry. Phys. Rev. D **102**, 035022 (2020). https://doi.org/10.1103/PhysRevD.102.035022. arXiv:2004.07863
11. Y. Jho, J.-C. Park, S.C. Park, P.-Y. Tseng, Leptonic new force and cosmic-ray boosted dark matter for the XENON1T excess. Phys. Lett. B **811**, 135863 (2020). https://doi.org/10.1016/j.physletb.2020.135863. arXiv:2006.13910
12. N. Okada, S. Okada, D. Raut, Q. Shafi, Dark matter Z' and XENON1T excess from $U(1)_X$ extended standard model. Phys. Lett. B **810**, 135785 (2020). https://doi.org/10.1016/j.physletb.2020.135785. arXiv:2007.02898
13. P. Van Dong, C.H. Nam, D. Van Loi, Canonical seesaw implication for two-component dark matter. Phys. Rev. D **103**, 095016 (2021). https://doi.org/10.1103/PhysRevD.103.095016. arXiv:2007.08957
14. P. Van Dong, Flipping principle for neutrino mass and dark matter. Phys. Rev. D **102**, 011701 (2020). https://doi.org/10.1103/PhysRevD.102.011701. arXiv:2003.13276
15. D. Van Loi, C.H. Nam, N.H. Tan, P. Van Dong, Dark charge versus electric charge. Phys. Rev. D **105**, 075012 (2022). https://doi.org/10.1103/PhysRevD.105.075012. arXiv:2004.06005
16. N. Okada, O. Seto, Dirac dark matter, dark radiation, and the type-II seesaw mechanism in alternative U(1)X standard model. Phys. Rev. D **105**, 123512 (2022). https://doi.org/10.1103/PhysRevD.105.123512. arXiv:2202.08508
17. E. Bertuzzo, S. Jana, P.A.N. Machado, R. Zukanovich Funchal, Neutrino masses and mixings dynamically generated by a light dark sector. Phys. Lett. B **791**, 210 (2019). https://doi.org/10.1016/j.physletb.2019.02.023. arXiv:1808.02500
18. A. Das, N. Okada, S. Okada, D. Raut, Probing the seesaw mechanism at the 250 GeV ILC. Phys. Lett. B **797**, 134849 (2019). https://doi.org/10.1016/j.physletb.2019.134849. arXiv:1812.11931
19. K. Asai, K. Hamaguchi, N. Nagata, S.-Y. Tseng, K. Tsumura, Minimal gauged U(1)$_{L_\alpha - L_\beta}$ models driven into a corner. Phys. Rev. D **99**, 055029 (2019). https://doi.org/10.1103/PhysRevD.99.055029. arXiv:1811.07571
20. A. Das, S. Goswami, K.N. Vishnudath, T. Nomura, Constraining a general U(1)$'$ inverse seesaw model from vacuum stability, dark matter and collider. Phys. Rev. D **101**, 055026 (2020). https://doi.org/10.1103/PhysRevD.101.055026. arXiv:1905.00201
21. P. Ghosh, S. Mahapatra, N. Narendra, N. Sahu, TeV scale modified type-II seesaw mechanism and dark matter in a gauged U(1)B-L symmetric model. Phys. Rev. D **106**, 015001 (2022). https://doi.org/10.1103/PhysRevD.106.015001. arXiv:2107.11951
22. E. Ma, D.P. Roy, S. Roy, Gauged L(mu) - L(tau) with large muon anomalous magnetic moment and the bimaximal mixing of neutrinos. Phys. Lett. B **525**, 101 (2002). https://doi.org/10.1016/S0370-2693(01)01428-9. arXiv:hep-ph/0110146
23. S. Baek, N.G. Deshpande, X.G. He, P. Ko, Muon anomalous g-2 and gauged L(muon)–L(tau) models. Phys. Rev. D **64**, 055006 (2001). https://doi.org/10.1103/PhysRevD.64.055006. arXiv:hep-ph/0104141
24. S. Baek, P. Ko, Phenomenology of U(1)(L(mu)-L(tau)) charged dark matter at PAMELA and colliders. JCAP **10**, 011 (2009). https://doi.org/10.1088/1475-7516/2009/10/011. arXiv:0811.1646
25. P. Van Dong, D. Van Loi, Asymmetric matter from $B-L$ symmetry breaking. Eur. Phys. J. C **80**, 1137 (2020). https://doi.org/10.1140/epjc/s10052-020-08693-2. arXiv:2001.03862
26. P. Van Dong, T.N. Hung, D. Van Loi, Abelian charge inspired by family number. Eur. Phys. J. C **83**, 199 (2023). https://doi.org/10.1140/epjc/s10052-023-11365-6. arXiv:2212.13155
27. D. Van Loi, C.H. Nam, P. Van Dong, Minimal model inspired by family number and dark matter. arXiv:2305.04681
28. P. Langacker, M. Plumacher, Flavor changing effects in theories with a heavy Z' boson with family nonuniversal couplings. Phys. Rev. D **62**, 013006 (2000). https://doi.org/10.1103/PhysRevD.62.013006. arXiv:hep-ph/0001204
29. E. Ma, Verifiable radiative seesaw mechanism of neutrino mass and dark matter. Phys. Rev. D **73**, 077301 (2006). https://doi.org/10.1103/PhysRevD.73.077301. arXiv:hep-ph/0601225
30. I.Z. Rothstein, K.S. Babu, D. Seckel, Planck scale symmetry breaking and majoron physics. Nucl. Phys. B **403**, 725 (1993). https://doi.org/10.1016/0550-3213(93)90368-Y. arXiv:hep-ph/9301213
31. S. Weinberg, Goldstone bosons as fractional cosmic neutrinos. Phys. Rev. Lett. **110**, 241301 (2013). https://doi.org/10.1103/PhysRevLett.110.241301. arXiv:1305.1971
32. P. Van Dong, Interpreting dark matter solution for $B - L$ gauge symmetry. arXiv:2305.19197
33. UTfit collaboration, Model-independent constraints on $\Delta F = 2$ operators and the scale of new physics. JHEP **03**, 049 (2008). https://doi.org/10.1088/1126-6708/2008/03/049. arXiv:0707.0636
34. G. Isidori, Y. Nir, G. Perez, Flavor physics constraints for physics beyond the Standard Model. Ann. Rev. Nucl. Part. Sci. **60**, 355 (2010). https://doi.org/10.1146/annurev.nucl.012809.104534. arXiv:1002.0900
35. F. Gabbiani, E. Gabrielli, A. Masiero, L. Silvestrini, A complete analysis of FCNC and CP constraints in general SUSY extensions of the standard model. Nucl. Phys. B **477**, 321 (1996). https://doi.org/10.1016/0550-3213(96)00390-2. arXiv:hep-ph/9604387
36. A.J. Buras, F. De Fazio, 331 models facing the tensions in $\Delta F = 2$ processes with the impact on ε'/ε, $B_s \rightarrow \mu^+\mu^-$ and $B \rightarrow K^*\mu^+\mu^-$. JHEP **08**, 115 (2016). https://doi.org/10.1007/JHEP08(2016)115. arXiv:1604.02344
37. A. Lenz, G. Tetlalmatzi-Xolocotzi, Model-independent bounds on new physics effects in non-leptonic tree-level decays of B-mesons.

JHEP **07**, 177 (2020). https://doi.org/10.1007/JHEP07(2020)177. arXiv:1912.07621

38. A.J. Buras, F. De Fazio, ε'/ε in 331 Models. JHEP **03**, 010 (2016). https://doi.org/10.1007/JHEP03(2016)010. arXiv:1512.02869

39. Flavour Lattice Averaging Group (FLAG) collaboration, FLAG Review 2021. Eur. Phys. J. C **82**, 869 (2022). https://doi.org/10.1140/epjc/s10052-022-10536-1. arXiv:2111.09849

40. A. Bazavov et al., B- and D-meson leptonic decay constants from four-flavor lattice QCD. Phys. Rev. D **98**, 074512 (2018). https://doi.org/10.1103/PhysRevD.98.074512. arXiv:1712.09262

41. P.V. Dong, H.N. Long, D.T. Nhung, Atomic parity violation in the economical 3–3–1 model. Phys. Lett. B **639**, 527 (2006). https://doi.org/10.1016/j.physletb.2006.06.077. arXiv:hep-ph/0604199

42. E. Golowich, J. Hewett, S. Pakvasa, A.A. Petrov, Implications of D^0 - $\bar{D}^0$ mixing for new physics. Phys. Rev. D **76**, 095009 (2007). https://doi.org/10.1103/PhysRevD.76.095009. arXiv:0705.3650

43. M. Carena, A. Daleo, B.A. Dobrescu, T.M.P. Tait, Z' gauge bosons at the Tevatron. Phys. Rev. D **70**, 093009 (2004). https://doi.org/10.1103/PhysRevD.70.093009. arXiv:hep-ph/0408098

44. ALEPH, DELPHI, L3, OPAL, LEP Electroweak collaboration, Electroweak measurements in electron-positron collisions at W-boson-pair energies at LEP. Phys. Rep. **532**, 119 (2013). https://doi.org/10.1016/j.physrep.2013.07.004. arXiv:1302.3415

45. E. Eichten, K.D. Lane, M.E. Peskin, New tests for quark and lepton substructure. Phys. Rev. Lett. **50**, 811 (1983). https://doi.org/10.1103/PhysRevLett.50.811

46. ATLAS collaboration, Search for high-mass dilepton resonances using 139 fb^{-1} of pp collision data collected at $\sqrt{s} =$ 13 TeV with the ATLAS detector. Phys. Lett. B **796**, 68 (2019). https://doi.org/10.1016/j.physletb.2019.07.016. arXiv:1903.06248

47. A.D. Martin, W.J. Stirling, R.S. Thorne, G. Watt, Parton distributions for the LHC. Eur. Phys. J. C **63**, 189 (2009). https://doi.org/10.1140/epjc/s10052-009-1072-5. arXiv:0901.0002

48. CMS collaboration, Search for resonant and nonresonant new phenomena in high-mass dilepton final states at $\sqrt{s} =$ 13 TeV. JHEP **07**, 208 (2021). https://doi.org/10.1007/JHEP07(2021)208. arXiv:2103.02708

49. G. Belanger, F. Boudjema, A. Pukhov, A. Semenov, Dark matter direct detection rate in a generic model with micrOMEGAs 2.2. Comput. Phys. Commun. **180**, 747 (2009). https://doi.org/10.1016/j.cpc.2008.11.019. arXiv:0803.2360

50. XENON collaboration, Dark matter search results from a one ton-year exposure of XENON1T. Phys. Rev. Lett. **121**, 111302 (2018). https://doi.org/10.1103/PhysRevLett.121.111302. arXiv:1805.12562

51. LZ collaboration, First dark matter search results from the LUX-ZEPLIN (LZ) experiment. Phys. Rev. Lett. **131**, 041002 (2023). https://doi.org/10.1103/PhysRevLett.131.041002. arXiv:2207.03764

52. XENON collaboration, Projected WIMP sensitivity of the XENONnT dark matter experiment. JCAP **11**, 031 (2020). https://doi.org/10.1088/1475-7516/2020/11/031. arXiv:2007.08796

53. LZ collaboration, Projected WIMP sensitivity of the LUX-ZEPLIN dark matter experiment. Phys. Rev. D **101**, 052002 (2020). https://doi.org/10.1103/PhysRevD.101.052002. arXiv:1802.06039

54. DARWIN collaboration, DARWIN: towards the ultimate dark matter detector. JCAP **11**, 017 (2016). https://doi.org/10.1088/1475-7516/2016/11/017. arXiv:1606.07001

55. V. Barger, W.-Y. Keung, G. Shaughnessy, Spin dependence of dark matter scattering. Phys. Rev. D **78**, 056007 (2008). https://doi.org/10.1103/PhysRevD.78.056007. arXiv:0806.1962

56. P. Junnarkar, A. Walker-Loud, Scalar strange content of the nucleon from lattice QCD. Phys. Rev. D **87**, 114510 (2013). https://doi.org/10.1103/PhysRevD.87.114510. arXiv:1301.1114

57. M. Hoferichter, J. Ruiz de Elvira, B. Kubis, U.-G. Meißner, High-precision determination of the pion-nucleon σ term from Roy–Steiner equations. Phys. Rev. Lett. **115**, 092301 (2015). https://doi.org/10.1103/PhysRevLett.115.092301. arXiv:1506.04142

58. PandaX-II collaboration, Results of dark matter search using the full PandaX-II exposure. Chin. Phys. C **44**, 125001 (2020). https://doi.org/10.1088/1674-1137/abb658. arXiv:2007.15469

59. LUX collaboration, Results from a search for dark matter in the complete LUX exposure. Phys. Rev. Lett. **118**, 021303 (2017). https://doi.org/10.1103/PhysRevLett.118.021303. arXiv:1608.07648

60. S. Bhattacharya, P. Poulose, P. Ghosh, Multipartite interacting scalar dark matter in the light of updated LUX data. JCAP **04**, 043 (2017). https://doi.org/10.1088/1475-7516/2017/04/043. arXiv:1607.08461

61. XENON collaboration, Constraining the spin-dependent WIMP-nucleon cross sections with XENON1T. Phys. Rev. Lett. **122**, 141301 (2019). https://doi.org/10.1103/PhysRevLett.122.141301. arXiv:1902.03234

62. PandaX-II collaboration, PandaX-II constraints on spin-dependent WIMP-nucleon effective interactions. Phys. Lett. B **792**, 193 (2019). https://doi.org/10.1016/j.physletb.2019.02.043. arXiv:1807.01936

63. LUX collaboration, Limits on spin-dependent WIMP-nucleon cross section obtained from the complete LUX exposure. Phys. Rev. Lett. **118**, 251302 (2017). https://doi.org/10.1103/PhysRevLett.118.251302. arXiv:1705.03380